DOI: 10.1070/RCR4663

Upconversion nanoparticles and their hybrid assemblies for biomedical applications

Ekaterina A. Grebenik,[a] Alexey B. Kostyuk,[b] Sergey M. Deyev [c, d]

[a] Institute for Regenerative Medicine, I.M.Sechenov First Moscow State Medical University ul. Trubetskaya 8, str. 2, 119991 Moscow, Russian Federation
[b] Institute of Biology and Biomedicine, National Research Lobachevsky State University of Nizhni Novgorod prosp. Gagarina 23, kor. 1, 603950 Nizhny Novgorod, Russian Federation
[c] M.M.Shemyakin and Yu.A.Ovchinnikov Institute of Bioorganic Chemistry, Russian Academy of Sciences ul. Miklukho-Maklaya 16/10, 117997 Moscow, Russian Federation
[d] National Research Tomsk Polytechnic University prosp. Lenina 30, 634050 Tomsk, Russian Federation

The progress in the design of hybrid photoluminescent assemblies based on upconversion nanoparticles (UCNPs) meant for biomedical applications is analyzed. The key approaches to the synthesis of bright UCNPs and their surface modification, including encapsulation into hydrophilic shells and providing with therapeutic and targeting agents, are described. The range of potential applications of UCNPs in analytical biochemistry, biomedical diagnostics and therapy of cancer and infectious diseases is considered.
The bibliography includes 145 references.

Contents

I. Introduction 1277
II. The mechanism of photoluminescence of upconversion nanoparticles 1278
III. Strategies for synthesis of upconversion nanoparticles 1279
IV. Surface modification of upconversion nanoparticles 1281
V. Detection of upconversion nanoparticle photoluminescence in living objects 1282
VI. Upconversion nanoparticles as optical contrast agents for biomedical applications 1284
VII. Self-assembled UCNP hybrids based on molecular adaptors 1287
VIII. Biocompatibility of upconversion nanoparticles 1288
IX. Therapeutic applications of upconversion nanoparticles 1290
X. Conclusion 1293

I. Introduction

In recent years, upconversion nanoparticles (UCNPs), which represent a new class of inorganic photoluminescent nanoparticles, have become highly popular in the biomedical community. Owing to their unique photophysical properties unknown in the living nature, they have attracted particular attention as contrast agents for optical medical diagnostics. The UCNP photophysics is

E.A.Grebenik. PhD in Biophysics, Leading Researcher at the IRM of the First MSMU.
E-mail: grebeneka@gmail.com
Current research interests: tissue engineering, molecular oncology, nanobiotechnology, fluorescence bioimaging.
A.B.Kostyuk. Junior Researcher at the IBBM UNN.
E-mail: kostyukalexey@mail.ru
Current research interests: nanobiotechnology, optical imaging, interaction of laser radiation with matter.

S.M.Deyev. Corresponding Member of the RAS, Doctor of Biological Sciences, Professor, Head of the Laboratory of Molecular Immunology at the IBCh RAS, Professor of the TPU.
Telephone: +7(499)724 – 7188, e-mail: deyev@ibch.ru
Current research interests: nanobiotechnology, molecular immunology, immunochemistry, enzymes, oncology.

Received 4 May, 2016
Translation: Z.P.Svitanko

© 2016 Russian Academy of Sciences and Turpion Ltd.

based on the upconversion, which implies transformation of the low-energy near-IR exciting radiation into higher-energy UV, visible or IR radiation.[1] For traditional dyes (fluorochromes), upconversion can be implemented upon multiphoton excitation, which requires high intensity of the exciting radiation and, hence, the use of expensive pulse lasers.[2] In the case of UCNPs, the upconversion mechanism is based on two- or multi-photon transitions that involve real energy levels and bring lanthanide ions into long-lived metastable states. This fact enables a considerable decrease in the exciting radiation intensity down to a level safe for biological systems[3,4] and, hence, it is possible to use cheap, easily available, continuous-wave operating lasers. Furthermore, the UCNP photoluminescence intensity is 6–8 times as high as intensity of the signal resulting from two-photon excitation of traditional fluorochromes; this increases the depth of optical probing of a biological tissue up to 3 cm and even more.[5]

The UCNP bioconjugates provided with molecules that play specialized functions in a living organism can act as targeted contrast or therapeutic agents. These structures are called hybrid as they combine components of inorganic (UCNP platform) and organic (biomolecule) nature. Depending on the biomolecule functions, UCNP bioconjugates are able to control the molecular traffic in the cells, participate in enzymatic transformations and perform targeted delivery to cellular and tissue structures for selective identification of lesions or neoplastic transformations and to exert therapeutic effect. The targeted delivery is accomplished *via* recognition of biological targets associated with a particular process in the body. A cellular tumour marker present in a large amount in the tumour tissue can serve as such target. The use of an inorganic UCNP platform makes it possible to detect tumour markers at a single-molecule level, which opens up new routes to the development of high-sensitivity methods for early non-invasive diagnosis of cancer. Furthermore, the possibility of selective interaction with biological targets and targeted delivery of biologically active factors opens up great prospects for the application of UCNPs in other areas of biomedical studies related to the development of therapeutic agents.

During the last decade, an enormous progress has been made in the development of UCNPs and their hybrids meant for biomedical practice. This subject is covered in numerous reviews. Some reviews deal with issues related to improvement of the physicochemical properties of UCNPs,[6,7] other consider the design of UCNP-based assemblies for diagnostic[8–11] and therapeutic[12–17] purposes. The present review integrates the material presented in the modern scientific literature concerning the key aspects of development of UCNP-based assemblies starting from optimization of the synthesis and bioconjugation processes and ending with the scope of their biomedical applications.

II. The mechanism of photoluminescence of upconversion nanoparticles

An upconversion nanoparticle is an inorganic oxide or fluoride nanocrystal doped with triply charged lanthanide ions of two types, that are, sensitizers and activators (in the formula, they are usually separated from the matrix material by a colon).[2,18] Sensitizer ions absorb radiation in the near-IR range and non-radiatively transfer the excitation energy to the neighbouring sensitizer ions or to activator ions. The interaction of the excited activator ion with the excited sensitizer ion brings about the upconversion process. As a result, the activator emits a photon with a higher energy compared with the absorbed single quantum of radiation.[19] The selection of various activator ions ensures the diversity of photoluminescence spectra programmed in the range from 450 to 1650 nm.[20]

Various types of UCNP compositions comprise $NaYF_4$:Yb,Er,[4,21,22] $NaYF_4$:Y,Yb,Er, Y_2O_3:Yb,Er,[23] SiO_2:Y,Yb,Er, SiO_2:Y,Yb,Tm,[19] ZrO_2:Yb,Er,[24] $NaScF_4$:Er,Yb,[25] Y_2O_3:Er,[26] LaF_3:Yb,Er,[27] YVO_4:Er, YVO_4:Er,Yb,[28] $CePO_4$:Tb@$LaPO_4$ (the character @ is used to separate the formulae of the core and the shell when applicable), LaF_3@Ln, $LaPO_4$@Ln,[29] $NaYbF_4$:Tm@CaF_2,[5] Y_2O_3:Er,[30] Gd_2O_3:Yb,Er,[32] $NaYF_4$:Yb,Nd,Er@$NaYF_4$:Nd,[31] $KGdF_4$:Yb,Er,[33] $NaLuF_4$:Gd,Yb,Er/Tm (Ref. 34) and so on. A long list of UCNPs of other compositions indicating spectral characteristics was reported in a summary table by Zijlmans *et al.*[19]

The fluoride matrix co-doped with ytterbium and erbium or thulium ($NaYF_4$:Yb,Er/Tm) has become most popular for the design of UCNPs for biomedical applications.[35,36] The $NaYF_4$ matrix is preferred owing to the high efficiency of upconversion,[37] and Yb^{3+} ions have high absorption cross-section at 980 nm and are capable of non-radiative transfer of excitation energy to activator ions (Er^{3+} and Tm^{3+}).[28] The energy conversion in the $NaYF_4$:Yb,Er UCNPs involves a cascade of complex processes (Fig. 1) initiated by absorption of long-wavelength (~980 nm) excitation light by Yb^{3+}. Then the excitation energy is non-radiatively transferred to the neighbouring Yb^{3+} or Er^{3+} ion, thus transmitting this ion to the metastable excited state. The excited Er^{3+} ion and one or more excited Yb^{3+} ions are capable of synchronous energy exchange and, as a result, the Er^{3+} ion is raised to a higher excited state and Yb^{3+} ion returns to the ground state. Thus, the excited Er^{3+} ion can emit photons in the visible[35,38] and UV ranges.[39] By varying the Er^{3+} concentration, it is possible to specify the ratio of photoluminescence intensity in different spectral regions (from green to red) and thus to obtain UCNPs with different spectral properties.[40] The excited $NaYF_4$:Yb,Tm UCNPs emit near-IR photoluminescence (~800 nm) upon sequential absorption of two photons or photoluminescence with a peak at 474 nm upon absorption of three photons.

The photoluminescence spectra of three types of UCNPs with the $NaYbF_4$ matrix doped with various activator ions (Er^{3+}, Ho^{3+} and Tm^{3+}) are shown in Fig. 2.

The diversity of photoluminescence spectra enables the simultaneous recording of signals coming from UCNPs with different composition; therefore, it is possible to study processes that occur in living objects in parallel. For example, several lymph nodes in a mouse body can be visualized (imaged) simultaneously by using UCNPs with different photoluminescence spectra. Figure 3 shows differentiated imaging of three lymph nodes 2 h after intradermal injection of three suspensions of UCNPs with different compositions based on

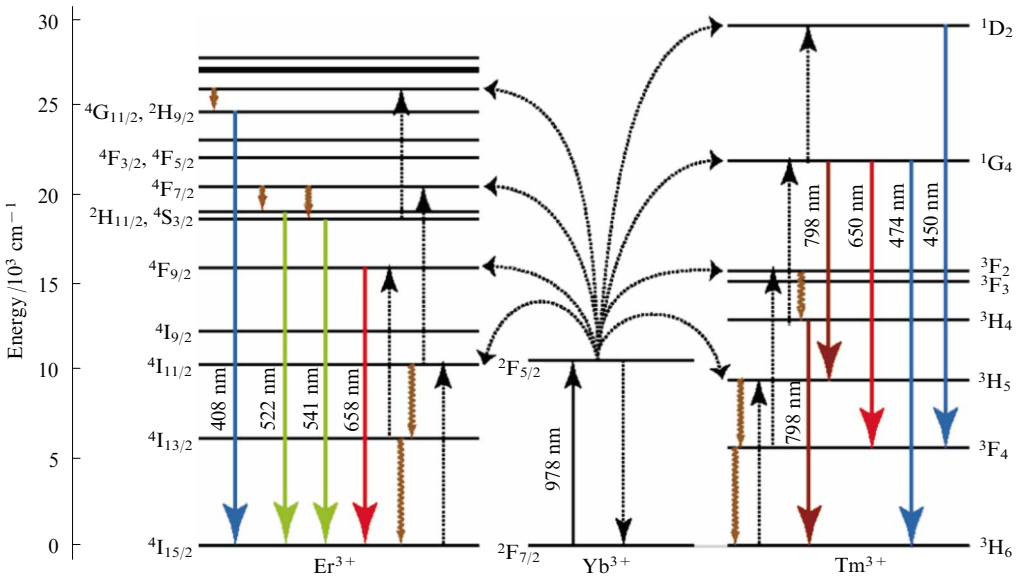


Figure 1. Diagram of energy levels and electron transitions of ytterbium ions (Yb^{3+}) involving erbium (Er^{3+}) or thulium (Tm^{3+}) ions in the $NaYF_4$:Yb,Er and $NaYF_4$:Yb,Tm UCNPs, respectively.[35]
The Yb^{3+} ion serves as the sensitizer and Er^{3+} and Tm^{3+} ions are activators. The dashed lines show the non-radiative energy transfer.

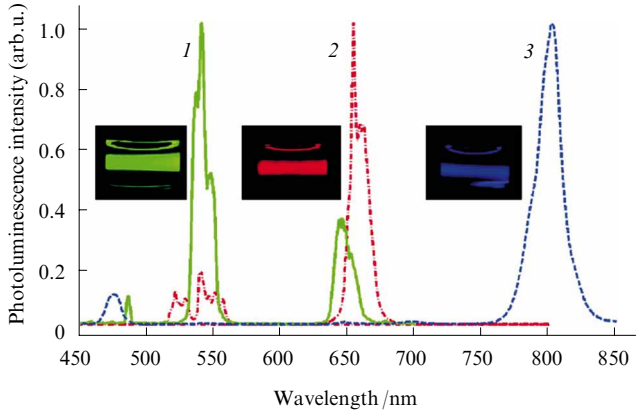


Figure 2. Photoluminescence spectra of colloid solutions of the $NaYbF_4$:Yb,Er (*1*), $NaYbF_4$:Yb,Ho (*2*) and $NaYbF_4$:Yb,Tm (*3*) UCNPs upon near-IR excitation.[38]

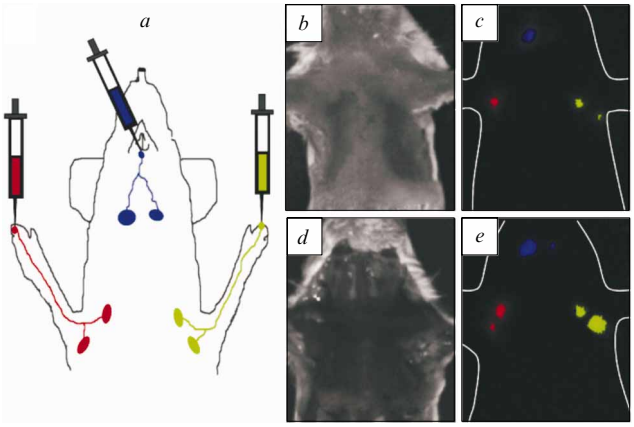


Figure 3. Differential imaging of lymph nodes in a mouse body using three UCNPs of different composition based on $NaYF_4$:Yb,Er/Tm.[40]
Schematic view of intradermal injection of UCNP suspensions (*a*); brightfield image of the mouse after injection of UCNP suspension (*b*); photoluminescence images of lymph nodes obtained 2 h after injection of UCNP suspension (*c*) and after autopsy (*e*); brightfield image of the mouse after autopsy (*d*).

$NaYF_4$:Yb,Er/Tm into the areas designated in Fig. 3 *a* and images taken after autopsy.[40]

III. Strategies for synthesis of upconversion nanoparticles

Upconversion nanoparticles with a specified size are often prepared using the standard two-stage method for growing fluoride crystals doped with lanthanide ions from solutions of organometallic compounds and oleic acid in an oxygen-free environment (thermal decomposition technique).[25, 41 – 43] The growth occurs with heating and continuous stirring of the reactants. This gives a powder of crystals with a hydrophobic oleic acid coating. The UCNP size varies from several nanometres to 1 μm.[44] The existing versions of this procedure are suitable for the preparation of UCNPs with pre-specified photophysical and morphological properties.

Apart from thermal decomposition, other methods for UCNP synthesis include combustion synthesis in solutions of metal nitrates and urea (fuel) initiated by the exothermic reaction between solution components after preliminary heating,[28] in particular, microwave heating;[45]

precipitation from solutions of metal salts with ammonia;[24] solvothermal synthesis,[2] which proceeds in high-boiling solvents at 120–350 °C *via* nucleation and growth; and hydrothermal synthesis,[33,37] which is performed at elevated pressure and temperature.

The activator concentration in UCNPs is, on average, 0.2 mol.%–0.5 mol.% and the sensitizer concentration is 20 mol.%–40 mol.%, which ensures the highest photoluminescence intensity upon excitation with a laser at 100 W cm^{-2} intensity. An increase in the activator concentration quenches the photoluminescence of UCNPs; this can be avoided only by excitation with high-intensity light. For excitation intensity of 2.5×10^6 W cm^{-2}, an increase in the Tm^{3+} concentration in the $NaYF_4$:Yb,Tm UCNPs to 8 mol.% was found to induce a 70-fold increase in the photoluminescence intensity. Therefore, it is possible to track even single UCNP particles with a sensitivity three orders of magnitude higher than that achieved with quantum dots.[46] However, such intensity levels are often inadmissible for biomedical practice as they lead to overheating of living tissues.

Despite a considerable progress in UCNP synthesis, the conversion efficiency (η_{uc}), which is defined as the ratio of the emitted photoluminescence power to the absorbed excitation power (W W^{-1}), has remained relatively low until recently, being markedly lower than η_{uc} of upconversion microparticles[29] (4% against 0.1% for UCNPs with an average diameter of 30 nm). The cause is that non-radiative energy relaxation through the surface starts to predominate with decreasing crystal size, thus suppressing upconversion.[21]

High η_{uc} values for UCNPs were achieved by optimization of the synthesis.[34] The primary product of synthesis is the crystalline compound with a cubic lattice, so-called α-phase, which has a low η_{uc} value. An additional high-temperature treatment in an oxygen-free environment in oleic acid transforms these crystals into another phase with a more closely-packed hexagonal crystal lattice[3,7] (β-phase), which rises the η_{uc} value by an order of magnitude.[21] The dependence of η_{uc} on the excitation intensity is non-linear (Fig. 4). Saturation occurs, most often, at an intensity of 10–1000 W cm^{-2} (Refs 22 and 47). The logarithmic dependence of the UCNP photoluminescence intensity on the excitation intensity attests to a two-photon absorption.[45]

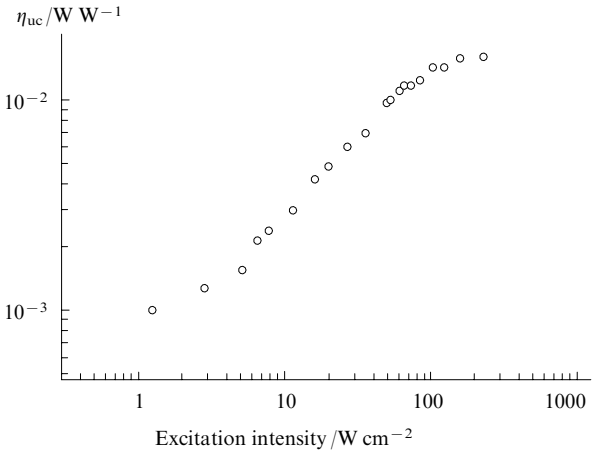


Figure 4. Conversion efficiency of the $NaYF_4$:Yb,Er UCNPs in the 500–700 nm spectral range *vs.* exciting intensity at 978 nm.[47]

It is noteworthy that UCNP photoluminescence is quenched almost inevitably in aqueous solutions because of the enhancement of multiphonon relaxation of excited lanthanide ions due to high energy of vibrational modes of water molecules.[48] The presence of functional groups and defects on the UCNP surface also promotes non-radiative relaxation of the absorbed energy.[49] It was found that photoluminescence intensity is directly dependent on the number of surface functional groups (CO_2, CH, NH_2, OH, *etc.*).[24] These problems can be partly solved by synthesis of two-layer core–shell particles.[50] This is achieved by coating the UCNP matrix doped with lanthanide ions with a protective layer (shell) of an undoped matrix[51] or a polymer material. After encapsulation of the $NaLuF_4$:Yb,Tm UCNPs into a $NaGdF_4$ shell, the photoluminescence efficiency at 800 nm increases 3.8-fold. Simultaneously, the excited state lifetime increases 1.7-fold.[52] The α-$NaYF_4$ shell results in a 50% higher green photoluminescence intensity of the β-$NaYF_4$:Yb,Er UCNPs.[34] The elimination of surface defects by coating a CaF_2 shell enhances the emission of $NaGdF_4$:Yb,Er by a factor of ~240.[49]

A beneficial effect of polymeric coatings on the photoluminescence of a UCNP aqueous colloid was found for polyacrylic acid (PAA), which reduced the effect of acidification on the photoluminescence intensity,[30] and for SiO_2, which not only suppressed quenching but also enhanced photoluminescence owing to activation of 'dormant' lanthanide ions on the UCNP surface by the complementary ligand field.[29]

The UCNP photoluminescence intensity can also be increased by depositing gold or silver layers on the particle surface. For example, the attachment of silver nanoparticles to a SiO_2-coated $NaYF_4$:Yb,Er UCNP surface entails, in some cases, a 14-fold enhancement of photoluminescence;[53] encapsulation of UCNP into a gold shell produces a 9.1-fold enhancement of green photoluminescence.[54] The increase in the UCNP photoluminescence intensity is caused by the fact that UCNPs coated with these metals experience the action of local electromagnetic fields. Furthermore, depending on the distance between the Au or Ag shell and UCNP, the photoluminescence of the particles is either enhanced or quenched. In the case of short distances and direct contact with the metals, UCNP emission is quenched because of the dominance of non-radiative energy transfer from UCNP to the metallic shell. The enhancement of photoluminescence is also accompanied by acceleration of radiative relaxation with the concomitant 1.5–2.4-fold shortening of the excited state lifetime.[54] Silica shell serves for separation of the UCNP from the Ag or Au layer. In an experiment using UCNP-SiO_2-Ag, the best photoluminescence enhancement was attained when the distance between the UCNP and silver nanoparticles was 10 nm; this distance was adjusted by varying the SiO_2 shell thickness. When the shell was >10 nm thick, the energy transfer was hampered and, hence, the photoluminescence enhancement effect was damped, whereas a decrease in the shell thickness led to photoluminescence

quenching as a result of energy transfer to silver nanoparticles.[53]

One more way of enhancing the UCNP photoluminescence is based on the matrix doping with some metal ions. The enhancement is attributed to the distortion of crystal field symmetry around the activator ions as a result of decreasing unit cell size or formation of vacancies in the matrix. A substantial photoluminescence enhancement was achieved by doping the UCNP matrix with Na^+, K^+, Zn^{2+} (Ref. 45), Sc^{3+}, Li^+ and Fe^{3+} (Ref. 55) ions. For example, doping of the $NaGdF_4$:Yb,Er UCNPs with Fe^{3+} ions taken in 30 mol.% concentration increased the photoluminescence intensity more than 30-fold.[55]

IV. Surface modification of upconversion nanoparticles

For successful use of UCNPs for biomedical purposes, in particular, in a living organism, their colloids should be stable in water under physiological conditions (*i.e.*, upon variations of pH, ionic strength and temperature) and the undesirable interactions with blood proteins and the toxic action on the whole body should be minimized.[56] However, UCNPs coated with a layer of hydrophobic oleic acid molecules can be dispersed only in organic solvents (hexane or chloroform). A series of methods for solving this issue have been developed, in particular, surface modification of UCNPs by hydrophilic agents or functionalization with chemically reactive groups (carboxyl, thiol, aldehyde, amino and other groups), which are meant to ensure the colloid stability in an aqueous medium and the possibility of further chemical modification.[2]

The displacement of oleic acid molecules from the UCNP surface by citric acid is the simplest surface modification method, which, moreover, does not affect considerably the particle size and morphology.[57] The colloid stability of the obtained material in aqueous and buffer solutions is provided by the carboxyl groups of citric acid. This shell is held on the UCNP surface *via* chelation of metal ions.[3, 52] A similar strategy was used to displace oleylamine molecules from the UCNP surface by 2-aminoethyl dihydrogen phosphate.[58] However, this modification induced a noticeable photoluminescence quenching. Thioacetic acid, which forms a strong S–Y bond on the UCNP surface without photoluminescence quenching, is the most attractive agent for ligand-exchange surface modification of UCNPs.[59] A drawback of this method is the presence of residual oleic acid molecules on the modified UCNP surface.

Some researchers propose a strategy for forming a hydrophilic shell during UCNP synthesis. In this case, hydrophilic polymers are used instead of oleic acid as surfactants that prevent crystals from uncontrolled growth. The requirements imposed on these polymers include thermal stability and the presence of charged groups. Wang *et al.*[60] developed a procedure for encapsulation of UCNP into a polyethyleneimine (PEI) shell. The amino groups present in PEI favour mutual repulsion of particles in an aqueous solution and allow for subsequent bioconjugation. However, toxic action of UCNP-PEI on living structures was reported. The incubation of osteoblast cells with UCNP-PEI in a relatively low concentration (50 μg ml^{-1}) for 24 h decreased the cell viability by 40%.[5] Furthermore, the high positive charge of UCNP-PEI results in their effective binding to the cells.[33, 61] Polyacrylic acid is a non-toxic alternative to PEI.[62, 63] Owing to numerous carboxyl groups, PAA-coated UCNPs are hydrophilic in aqueous solutions. PAA can be attached to UCNPs either during the synthesis or after the removal of oleic acid on treatment with nitrosonium tetrafluoroborate ($NOBF_4$).[5, 64] One more way of PAA functionalization of UCNPs consists in preliminary modification of PAA with octylamine residues able to intercalate into the oleic acid and octadec-1-ene layer on the surface of as-synthesized UCNPs.[65] It is noteworthy that in some cases, the use of PAA affects the photoluminescence spectrum of UCNPs by shifting it to longer wavelengths,[51] and the PEI coating decreases the long-wavelength photoluminescence intensity.[33]

The optimal method for the surface modification of UCNPs is encapsulation of hydrophobic UCNPs into an additional hydrophilic shell using organic polymers or organosilicon compounds.

The simplest procedure for encapsulation of UCNPs into a polymer shell is layer-by-layer modification with polyelectrolytes. The procedure is based on van der Waals interaction of charged polymers with the particles and with one another. Wang *et al.*[66] developed a scheme of coating of UCNPs with positively charged poly(allylamine hydrochloride) (PAH) and negatively charged poly(styrene sulfonate) (PSS). The polyelectrolytes are alternately deposited under optimized conditions. The coating thickness can be varied by changing the number of deposited layers. For example, upon coating of UCNPs of diameter 50 nm with one layer of PAH and its negatively charged derivative with succinic anhydride, the UCNP diameter became 59 nm; after deposition of two layers, the diameter became 80 nm and with three layers, it was 140 nm.[67] Coating with four PAH/PSS polyelectrolyte layers increased the UCNP diameter from 100 to 120 nm, and after coating with eight layers, it was 140 nm.[32] However, the intensity of UCNP photoluminescence noticeably decreased with increasing the number of layers. The authors attributed this trend to the effect of inorganic groups.[32] In addition, the subsequent modification and application directly in a biological medium are often associated with severe variations of the pH, which may induce the loss of the polyelectrolyte layer and aggregation.

A SiO_2 shell endows UCNPs with a fairly high stability over a broad pH range;[68] however, this shell substantially increases the particle size. The SiO_2 shell is deposited[69] by the Stöber process comprising hydrolysis and polycondensation of tetraethoxysilane in the presence of amines after attachment of tetraethoxysilane alkyl groups to the hydrophobic chains of oleic acid on the UCNP surface.[70] In some cases, modification is carried out in a water–oil emulsion.[71] The silanol groups ensure the hydrophilicity and the possibility of bioconjugation. If necessary, the UCNP-SiO_2 obtained in this way can be functionalized by surface amino groups on treatment with (3-aminopropyl)trimethoxysilane[55, 69, 72] or (3-aminopropyl)triethoxysilane.[20]

Guller *et al.*[73] used even larger structures with UCNP inclusions — so-called polystyrene microspheres. They were obtained by styrene polymerization in the presence

of poly(*N*-vinylpyrrolidone). Encapsulation of UCNPs into polyacrolein microspheres *via* partial displacement of oleic acid molecules from the UCNP surface by tetramethylammonium hydroxide, which initiates polymerization of hydrophilic acrolein molecules, has also been proposed.[74] The stability of the ready particles in a colloid system was maximized by using the radical initiator $K_2S_2O_8$, which cross-linked the surface acrolein residues at the C=C double bonds. However, despite low cytotoxicity found in human HaCaT keratinocytes, the large size of the microspheres (260 nm) obtained by this method restricts the scope of applicability of the particles in the biomedical practice.[74]

Amphiphilic polymers containing both hydrophobic and hydrophilic chains serve as an alternative to a SiO_2 coating. Owing to the hydrophobic interaction, the amphiphilic polymer covers the UCNP surface, while hydrophilic chains provide the stability of the resulting structures in aqueous solutions for a period of up to 1 month.[75] The cross-links between polymer molecules account for the integrity of the whole shell. When the amphiphilic poly(maleic anhydride-*alt*-1-octadecene) (PMAO) copolymer is used, the alkyl chains are inserted between the oleic acid molecules on the UCNP surface, whereas the anhydride adds water to form charged carboxyl groups, which maintain the colloid stability in the aqueous medium and can serve for the subsequent bioconjugation.

One more group of methods for the surface modification of UCNPs is based on reactions with oleic acid at the C=C double bonds. Peroxide epoxidation of oleic acid molecules on the UCNP surface cleaves the double bond to enable the attachment of hydrophilic polymers, as was demonstrated for polyethylene glycol (PEG) monomethyl ether[76] and polyhedral oligomeric silsesquioxane.[77] As a result, particles acquired colloid stability in an aqueous medium and almost complete biocompatibility in high doses, while their size increased insignificantly. The simultaneous double bond cleavage in oleic acid and formation of carboxyl groups are accomplished by using a combination of potassium permanganate with sodium metaperiodate (Lemieux – von Rudloff reagent). Sodium metaperiodate acts as the key oxidant, while potassium permanganate serves as the catalyst. This procedure gives UCNPs coated with azelaic acid with retention of the morphology, size and photoluminescence properties.[78]

The presence of salts in the biological and buffer systems results in shielding of the surface charge of nanoparticles; this suppresses the electrostatic repulsion and causes pronounced aggregation. Therefore, for living objects, coatings of inert PEG molecules,[65] which prevent particles from approaching one another and suppress the formation of aggregates,[26] are used most often. PEG-based polymers have low toxicity and are not immunogenic[50] and they increase the circulation time in the blood stream, which is very important for the systemic application of the agents.[79, 80] However, this approach is rather expensive and requires thorough optimization of the conditions of synthesis and quality control of the target product.

In recent years, increased attention has been drawn to approaches to UCNP modification that imply the use of natural materials (DNA, proteins, chitosan), which are distinguished by high biocompatibility, biodegradability and availability. For example, DNA can displace oleic acid from the UCNP surface as a result of chelation of lanthanide ions by phosphate groups. Free phosphate groups impart a high negative charge to the UCNPs, thus promoting high colloid stability in an aqueous medium.[81] Other examples are provided by the amphiphilic chitosan derivatives, which are attached to an oleic acid layer on the UCNP surface,[37, 82] and microspheres formed by the molecules of denatured glutaraldehyde-cross-linked human serum albumin.[83]

V. Detection of upconversion nanoparticle photoluminescence in living objects

Owing to the unique photophysical properties, which provide UCNPs with a number of advantages over the traditionally used fluorescent proteins and organic dyes, these nanoparticles are an excellent tool for highly sensitive visualization of biological targets. The key advantages include almost autofluorescence-free detection in living objects[37] due to prolonged photoluminescence with a shift to shorter wavelengths, in particular, in the visible and near-IR ranges; narrow photoluminescence peaks (25 – 50 nm wide) separated from the absorption region by at least 200 nm;[19] excitation by wavelengths (~980 nm) that fall in the biotissue transparency window;[75] stability against photobleaching[37, 84] and chemical degradation;[85] and the absence of phototoxic effect towards living objects.[3, 86, 87] The possibility of synthesis of UCNPs of exceptionally small size (< 5 nm)[64] in combination with the absence of blinking effect inherent in quantum dots and nanodiamonds and with the presence of a multitude of photoluminescence centres (up to several thousand)[2] provide the possibility of tracing even single target molecules using these nanocrystals.

V.1. Upconversion in the biotissue transparency window

The programmability of spectral characteristics of UCNPs makes it possible to prepare UCNPs with photoluminescence in the biotissue transparency window (with a maximum at about 800 nm for $NaYF_4$:Yb,Tm) in which light transmission through a biotissue is accompanied by minimal absorption and scattering losses. This is caused by the fact that radiation absorption by a biotissue is mainly associated with the presence of haemoglobin, oxy-haemoglobin (in the visible and UV ranges) and water (in the IR range), and scattering is minimal in the 700 – 1300 nm range.[35] Figure 5 shows the optical absorption spectra of water, haemoglobin and oxy-haemoglobin and the effective attenuation of the transmitted light in the human skin calculated with allowance for the optical absorption by predominant chromophores and the scattering effect.

As can be seen in Fig. 5, the UCNP excitation region (~980 nm) is matched by high water absorption level, which may lead to undesirable tissue heating. Therefore, in some cases, either excitation at shorter wavelengths is used[38] or UCNPs are doped with Nd^{3+} ions, which function as sensitizers (for example, in $NaYF_4$:Yb,Nd,Er@$NaYF_4$:Nd), enabling efficient excitation of UCNPs at 730, 808 and 865 nm.[31]

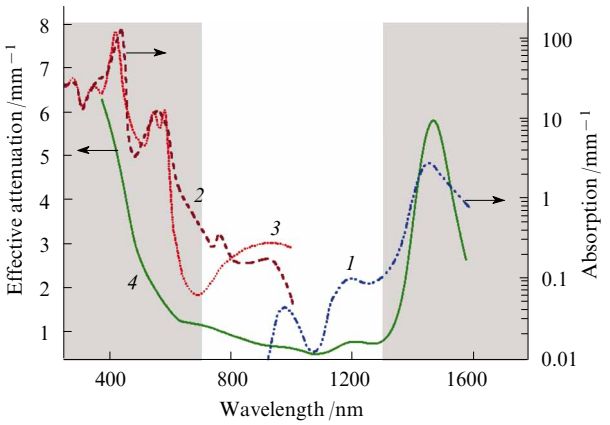


Figure 5. Optical absorption spectra of water (*1*), haemoglobin (*2*), oxy-haemoglobin (*3*) and effective light extinction spectrum in human skin (*4*).[35]
The transparency window in the biotissue is between 700 and 1300 nm.

V.2. Elimination of the background noise

The excitation of UCNPs in the near-IR range induces only a negligible fluorescence response of the biotissue (autofluorescence),[4] which considerably increases the contrast of imaging of UCNPs against the background of cellular or tissue structures.[23, 34, 35, 47] The background noise from the exciting radiation is efficiently suppressed by using filters, owing to the large gap between the optical absorption and emission ranges (up to 330 nm for $NaYF_4$:Yb,Er). As a result, UCNPs are markedly superior to organic molecular fluorochromes in the signal to noise ratio. For example, at a depth of 3 mm in a living tissue, this ratio is 12 times higher for UCNPs than for sodium fluorescein.[88]

A number of studies were aimed at achieving high-contrast photoluminescence images of UCNPs in living objects. Shan *et al.*[72] reported the detection of signals coming from a single UCNP in mouse mesothelioma AB12 cells. Background-free detection of UCNP signals

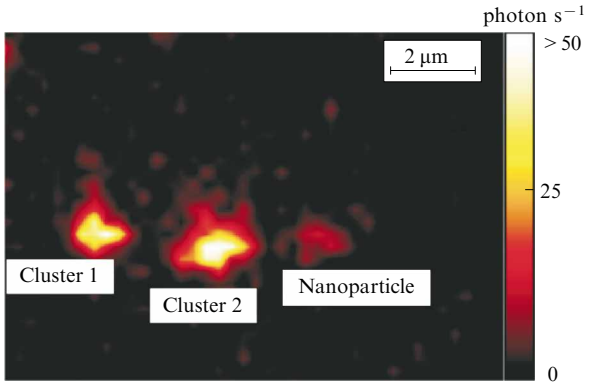


Figure 6. Image of single and clusterized UCNP particles in a drop of human lysed blood taken under epiluminescence microscope upon excitation at ~980 nm.[47]

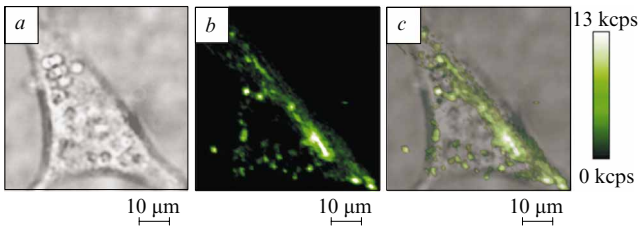


Figure 7. Image of UCNPs in a living cell of NIH 3T3 murine fibroblast taken by scanning laser confocal microscopy.[3]
(*a*) In the transmitted light, (*b*) upon excitation with near-IR radiation, (*c*) overlay. 1 kcps = 1000 photon s^{-1}.

in vitro was also demonstrated for histological sections of organs of mice intravenously injected with UCNPs[89] and within human skin samples.[35] Figure 6 shows the signal from a single UCNP in a lysed blood drop detected by Nadort *et al.*[47] by using epiluminescence microscopy. Apart from the single nanoparticle, the image shows two UCNP clusters.

Detection of single particles is often difficult because of the presence of large UCNP clusters in the sample; they enhance the background noise by scattering the photoluminescence. The use of laser scanning confocal microscopy reduces the background noise and, hence, provides images of a single UCNP in a living cell in the presence of large clusters (Fig. 7).[3] However, this method is time-consuming.

The final suppression of the background noise and biotissue autofluorescence can be achieved without using time-consuming optical methods and expensive interference filters by implementing the time-gated detection scheme.[90] According to this scheme, the photoluminescence signal of UCNPs that have much longer excited state lifetimes (~1 ms)[20] than typical endogenous fluorochromes (~3 ns) is detected after a specified period of time (~10 μs) upon a short-term excitation with a laser pulse.[2] This approach provides a considerable increase in the image contrast at the level of a single nanoparticle in a biological environment. Figure 8 shows the image of UCNP bioconjugates linked to sodium channels in frog cardiac myocytes; the image was obtained by measuring

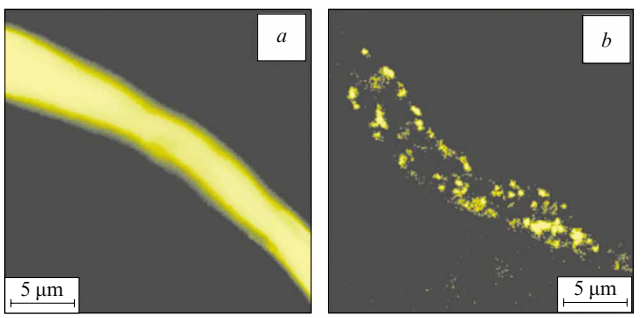


Figure 8. Photoluminescence images of UCNP bioconjugates linked to sodium and potassium channels of frog cardiac myocytes obtained before (*a*) and after (*b*) application of the time-gated detection scheme.[91]

the photoluminescence in the time interval from 10 to 80 μs after completion of the excitation. As a result, autofluorescence of cardiac myocytes and exciting radiation scattering were eliminated, and this increased the sensitivity of the method to the level of a single particle bound to a sodium channel.[91]

V.3. Stability against photobleaching

The use of fluorescence diffuse optical tomography to visualize UCNP-contrasted biological targets, in particular, cancer tumours *in vivo* can give images at a depth of up to 2 cm.[38] Visualization of biological targets located at larger depths in living objects is hampered due to scattering of transmitted light by structures of the biological tissue and to limitation of the maximum allowable level of the exciting radiation intensity. The radiant exposure of living human skin at a wavelength of ~980 nm should not exceed 700 W cm^{-2} during 1 ms.[47,92] However, since UCNPs have relatively low η_{uc} values, the detection of their weak signals requires a high-power laser. To maintain the maximum allowable doses, the laser beam is focused on the UCNP location site and the specified area is scanned similarly to how it is done in laser scanning confocal microscopy; alternatively, excitation radiation is supplied as nanosecond pulses. Furthermore, the use of high-power lasers, which are detrimental for organic fluorochromes, does not have a significant influence on the photoluminescence properties of UCNPs owing to low energy of photons in the UCNP matrix.[20] Figure 9 shows a comparative illustration for the photostability of UCNPs and organic fluorochromes — 3,3,3′,3′-tetramethyl-1,1′-bis(octadecyl)-indocarbocyanine perchlorate (DiI) and 4′,6-diamidino-2-phenylindole dichydrochloride (DAPI). The cells contrasted by UCNPs, DiI (cytoplasm) and DAPI (nucleus) were exposed to high-intensity (~4.6×10^6 W cm^{-2}) laser radiation at 405, 543 and 980 nm wavelengths for a long period of time (400 s). As a result, the fluorescence intensity decreased by 97.5% for DiI, by 99% for DAPI and by only 4% for UCNPs.

After continuous excitation of UCNPs with a 0.5 W laser at 980 nm for 7 h, the photoluminescence intensity was 95.6% of the initial value.[93]

V.4. Upconversion nanoparticles with magnetic properties

The presence of seven unpaired electrons in the 4f orbitals of Gd^{3+} ions accounts for paramagnetic behaviour of the Gd_2O_3,[32] $NaGdF_4$ (Ref. 49 and 98) and $KGdF_4$ (Ref. 33) matrices; therefore, UCNPs can be used as contrast agents in the NMR-based techniques. One more example of UCNPs with magnetic properties is Mn^{2+}-doped $NaYF_4$:Yb,Er,Mn UCNPs.[67] The contrast-enhanced NMR diagnosis substantially increases the maximum depth of detection of lesions and provides information about the three-dimensional structure of objects.

VI. Upconversion nanoparticles as optical contrast agents for biomedical applications

Highly sensitive detection of UCNPs in a noise-free mode has previously been achieved both for cell cultures *in vitro* [3,44,94,95] and for model animals *in vivo*.[38,95,96]

VI.1. Detection of photoluminescence of upconversion nanoparticles *in vivo*

An early study devoted to autofluorescence-free detection of UCNP signals in an animal body was based on the use of a glass capillary filled with a colloid solution of aminated Y_2O_3:Yb,Er UCNPs placed in the mouse oesophagus.[23] In another study, a suspension of UCNP-PEI (100 μl; 4.4 mg ml^{-1}) was intramuscularly injected in Wistar rats to a depth of 10 mm with subsequent non-invasive signal detection.[84] Some papers report imaging of UCNPs in their accumulation sites in a mouse body after intravenous injection. For example, signals of UCNPs encapsulated into polyacrolein microspheres were detected in the mouse liver, lungs and spleen 1 h after intravenous injection.[74] The radiation was detected using an electron multiplying charge coupled device (EMCCD camera).

Analysis of the literature devoted to the use of UCNP-based contrast agents in biomedical investigations shows that the interest in UCNPs is mainly focused on visualization of malignant lesions. The principle of visualization relies on the ability of nanoparticles to be accumulated in the tumour tissue owing to the specific structure and functional state of its blood vasculature.[97,98] The second factor that affects the accumulation of nanoparticles in the tumour tissue is formation of new blood vessels — neoangiogenesis, which is inherent in solid tumours of >1 mm^3 size and associated with malignancy.[52,99]

The first imaging of model tumours (xenografts) using UCNPs was reported by Nyk *et al.*[95] The mouse xenograft models of the human pancreatic cancer were visualized upon intravenous injection of UCNPs modified with 3-mercaptopropionic acid. The same principle was used

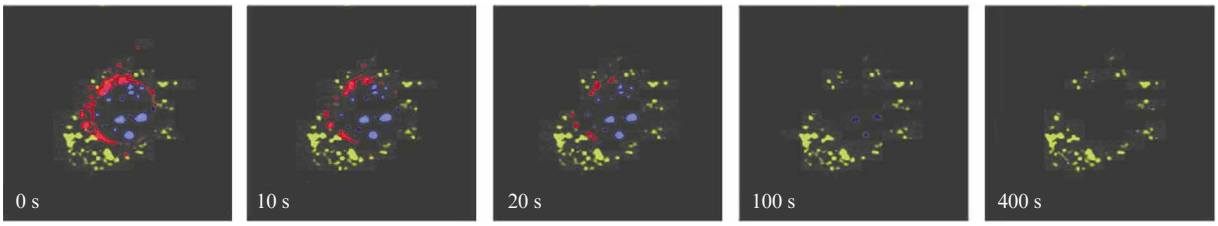


Figure 9. Photoluminescence images of a cell contrasted with UCNPs and organic fluorochromes, DiI (cytoplasm) and DAPI (nucleus), before irradiation and after 10, 20, 100 and 400 s of exposure to high-intensity laser radiation (~4.6×10^6 W cm^{-2}) at 405, 543 and 980 nm wavelengths.[4]

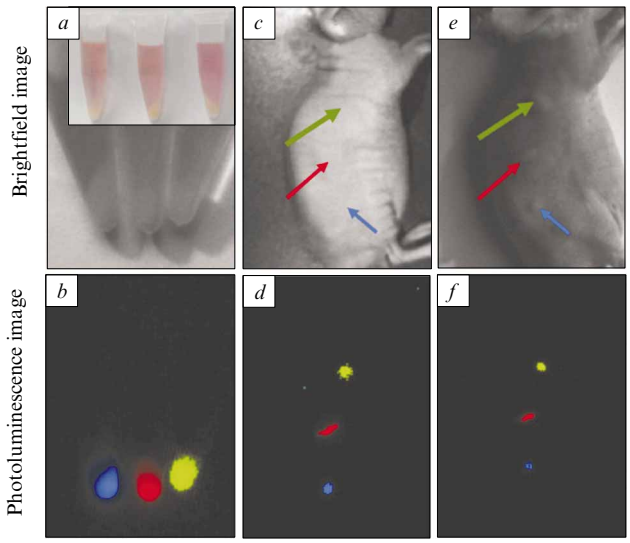


Figure 10. Visualization of formation of mouse xenograft models of human nasopharyngeal epidermoid carcinoma KB after implantation of cells with inclusion of three different UCNPs based on $NaYF_4$: Yb,Er/Tm.[40]
Brightfield images of cell suspensions (*a*), the mouse immediately after implantation (*c*) and the mouse a week after implantation (*e*); corresponding photoluminescence images (*b*, *d*, *f*).

in another study [52] to visualize the angiogenesis of mouse xenograft models of human nasopharyngeal epidermoid carcinoma KB.

The ability of UCNPs to be retained in living cells for long periods makes them a perfect tool for visualization of stem cell transplantation and tumour formation. It was found that after UCNP-PEI internalization, the mesenchymal stem cells continue to differentiate into osteoblasts and adipocytes, while retaining the UCNPs for at least 14 days.[5] The monitoring of UCNP-SiO_2-contrasted single mouse skeletal myoblasts in the blood stream was demonstrated in experimental damaged muscle regeneration in a mouse hind limb.[100] The tumour formation imaging was studied for mouse subcutaneous xenografts grown from human nasopharyngeal epidermoid carcinoma KB cells with inclusion of three different UCNP compositions based on $NaYF_4$: Yb,Er/Tm coated with an amphiphilic polymer.[40] Figure 10 shows simultaneous visualization of three xenografts with different optical properties.

VI.2. Hybrid assemblies of upconversion nanoparticles for targeted delivery

The use of hybrid assemblies of UCNPs loaded with targeted delivery agents is of high applied value for the development of immunoassay methods, DNA diagnostics and diagnostics of cancer.[2] These assemblies are able to recognize and identify biological targets, including single DNA and protein molecules (*e.g.*, membrane receptors), and structures embedded deep in biological tissue.[38, 79, 91, 101] The targeted delivery agents can be attached by direct physisorption methods [19] or covalent binding,[102 – 104] often with participation of cross-linking agents. Apart from the target recognition function, bioconjugation endows UCNPs with an additional stability in buffer solutions.

Among targeted delivery agents, antibody (immunoglobulin) molecules in various forms are used most often.[102 – 106] Several papers are devoted to UCNP targeting towards a tumour marker — HER2/neu receptor, which attracts attention because of the discovered relationship between the expression level of this receptor in the tumour and the clinical picture. Most of the relevant studies were performed using the human breast adenocarcinoma SK-BR-3 cells, which overexpress HER2/neu, and full-size anti-HER2/neu antibody attached to UCNPs *via* covalent bond.[102 – 104] Grebenik *et al.*[75] designed single-chain scFv antibody fragments (mini-antibody) for targeting UCNPs to HER2/neu.

Zhan *et al.*[38] used an anti-carcinoembryonic antigen antibody sorbed on the UCNP surface to visualize the human cervical carcinoma HeLa cells.

A number of publications present data on successful bioconjugation of UCNPs with folic acid (FA) to visualize the tumour cells that overexpress the FA receptor, including the *in vitro* cultured human lung cancer H460 cells,[107] human nasopharyngeal epidermoid carcinoma KB cells,[96, 108 – 110] human colon adenocarcinoma HT29 cells, human ovarian carcinoma OVCAR3 cells,[84] human cervical carcinoma HeLa cells,[37, 55, 111] human hepatoma Bel-7402 cells and mouse sarcoma S180 cells,[82] as well as human cervical carcinoma HeLa xenografts,[112] mouse hepatocellular carcinoma Hepa1-6 allografts [111] and so on. Figure 11 shows the confocal images of the HeLa cells after treatment with UCNP($NaYF_4$: Yb,Tm,Er)-FA bioconjugates upon excitation with a laser at 980 nm and the corresponding images in the transmitted light.[37]

The targeted delivery of UCNP – FA *in vivo* is accomplished by intravenous injection of a colloid solu-

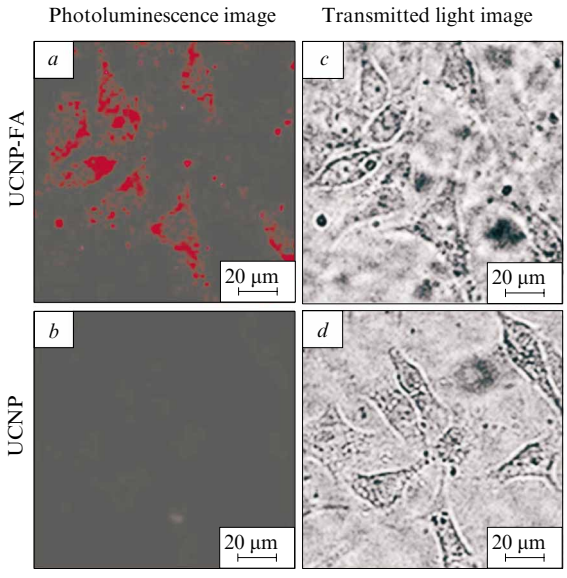


Figure 11. Photoluminescence images of human cervical carcinoma HeLa cells treated with UCNP-FA bioconjugates (*a*) and UCNPs (*b*) in 75 μg ml^{-1} concentration upon excitation with a laser at 980 nm and cell images in the transmitted light (*c* and *d*).[37]

tion of bioconjugates. After this, the signal from UCNPs located in the tumour area is detected. The introduction of free FA molecules in a concentration of 10 mg kg^{-1} together with the bioconjugates reduces the UCNP accumulation in the tumour by an order of magnitude.[112] The accumulation level of UCNP–FA bioconjugates in the tumour was increased by physisorption on the UCNP surface of the microtubulin inhibitor CA4P, which enhances the penetration into the tumour tissue.[88]

The cyclic tripeptide RGD (arginine-glycine-asparagine) is used as the targeted delivery agent for selective binding of UCNPs to the tumour cells that overexpress $\alpha_v\beta_3$ integrin receptor, which is a tumour marker playing a key role in the angiogenesis[112] and metastasis. The efficiency of UCNP–RGD bioconjugate targeting on the $\alpha_v\beta_3$ integrin receptor was demonstrated in experiments *in vitro* with human glioblastoma U87-LUC (Ref. 83) and U87MG cells.[65, 113, 114] Targeting of $NaYF_4$:Yb,Er,Tm-RGD to cancer cells *in vivo* was achieved by Xiong *et al.*[79] in nude mice experiments. The accumulation of particles in the human glioblastoma U87MG xenograft with high content of the $\alpha_v\beta_3$ integrin receptor was ~24 times as high as that in the human breast cancer MCF-7 xenograft devoid of the $\alpha_v\beta_3$ integrin receptor. Figure 12 shows the ratio of the UCNP accumulation levels in the two tumours and in organs of test animals, determined by measuring the Y^{3+} concentrations 24 h after the intravenous injection of UCNP–RGD.

Recently, the $NaYF_4$:Yb,Er,Ce UCNPs conjugated with recombinant chlorotoxin — a frequently occurring peptide neurotoxin synthesized in many types of cancer cells — were used to visualize the mouse xenograft models of rat glioma C6. The results demonstrated selective capture of bioconjugates by tumour cells.[115] The bioconjugation of $NaScF_4$:Er,Yb with the amino-terminal fragment of urokinase plasminogen activator allowed targeting UCNPs to the human lung cancer H1299 cells, overexpressing the tumour marker — urokinase plasminogen activator receptor.[25]

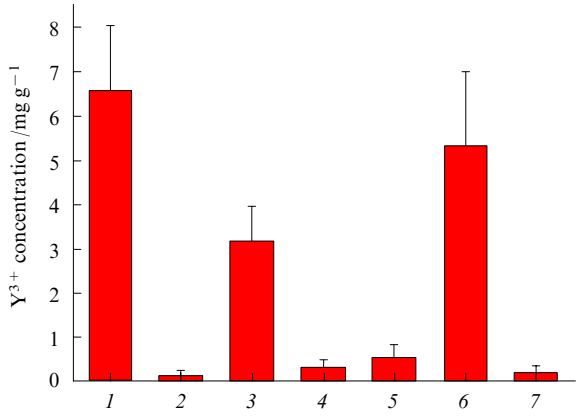


Figure 12. Concentration of Y^{3+} ions in mouse xenograft models of human glioblastoma U87MG and breast cancer MCF-7 and in mouse organs 24 h after intravenous injection of UCNP-RGD.[79] (*1*) U87MG xenograft, (*2*) MCF-7 xenograft, (*3*) spleen, (*4*) heart, (*5*) lungs, (*6*) liver, (*7*) kidneys.

Beaurepaire *et al.*[91] reported visualization of the sodium channels in frog cardiac myocytes involving the UCNP hybrid assemblies. The guanidine groups able to block voltage-gated sodium channels were used for targeted delivery (see Fig. 8). The selectivity of interaction with the target was confirmed by competitive inhibition of sodium channel binding in the presence of saxitoxin in a concentration of 15 nmol $litre^{-1}$.

VI.3. The use of upconversion nanoparticle-based hybrid assemblies in analytical techniques

Unlike natural supramolecular structures and many organic contrast agents, hybrid assemblies based on inorganic nanoparticles have a high physical strength and stability against corrosive environments; therefore, they can be quantitatively determined in tissues.

An UCNP-based method has been developed for quantitative determination of extremely low concentrations ($\geqslant$1 fmol $litre^{-1}$) of the early marker for breast cancer, miR-21 micro-RNA, in blood serum. The principle of the method is that the DNA hairpin containing a miR-21-complementary sequence, immobilized on a plate, is opened in the presence of miR-21. Hairpin opening results in the release of DNA sites to which the chain addition of UCNP-bound DNA sequences then takes place. The intensity of the UCNP signal from the sample is used to calculate the miR-21 concentration.[41]

Bioconjugates of UCNPs have also found use in the design of new-generation sensors for quantification of antibiotics with a sensitivity 50 times exceeding that of the traditional enzyme immunoassay. Hu *et al.*[116] developed a two-component system for determination of the concentration of norfloxacin, a broad spectrum antibiotic. The system consisted of the $NaYF_4$:Yb,Er UCNPs conjugated with a monoclonal anti-norfloxacin antibody and polystyrene particles coated with the norfloxacin–ovalbumin conjugates. The UCNP–anti-norfloxacin bioconjugates interact with norfloxacin both in the test sample and on the surface of polystyrene particles to give complexes; after that, complexes with polystyrene particles are precipitated and resuspended, and their concentration in the solution is determined from the UCNP photoluminescence intensity. An increase in the concentration of norfloxacin in the sample leads to inhibition of the binding to polystyrene particles and, hence, the photoluminescence intensity of the precipitate decreases. This approach accelerates and simplifies the assay and reduces its cost.[116]

A highly sensitive temperature nanosensor was designed using UCNP-SiO_2 and the hydrophobic fluorescent $Eu(TTA)_3(TPPO)_2$ complex (TTA is thenoyltrifluoroacetone, TPPO is triphenylphosphine oxide). The complex $Eu(TTA)_3(TPPO)_2$ was incorporated in the boundary layer between the UCNP and the SiO_2 shell during the surface modification. The intensity of photoluminescence of the nanosensor combining complementary lanthanide ions with anti-Stokes (Er^{3+}) and Stokes (Eu^{3+}) emission varied upon minor variations of the environment temperature.[70]

VII. Self-assembled UCNP hybrids based on molecular adaptors

The use of molecular adaptors — mutually complementary biomolecules — as linkers for UCNP bioconjugation provides structures with diversified combinations of components. The versatile strategy of self-assembly of UCNP bioconjugates consists in the following: one adaptor molecule is attached to the surface of UCNP, while the other one is linked to the functional agent (*e.g.*, the targeted delivery agent) or another nanoparticle. The final assembly may be performed either in advance or at the instant of interaction with the biological target by successive treatment of the test sample first with the recognition (targeted delivery) agent and then with the contrast (UCNP) modules.

Examples of molecular adaptors are the pairs antigen – antibody [dissociation constant (K_d) of the complex is $\sim 10^{-7} - 10^{-11}$ mol litre^{-1}],[117, 118] (strept)avidin – biotin ($K_d \sim 10^{-15}$ mol litre^{-1}),[118] barnase – barstar ($K_d \sim 10^{-14}$ mol litre^{-1})[119] and complementary DNA sequences.

VII.1. Complementary DNA sequences

The self-assembly of UCNP structures based on DNA strand complementarity has found use in the development of new methods of DNA diagnostics. Ma *et al.*[69] described the DNA diagnostics of salmonellosis based on the UCNP photoluminescence quenching *via* the resonance energy transfer to gold nanoparticles. Gold nanoparticles and UCNP-SiO_2 were loaded with single-stranded DNA molecules complementary to DNA sites of *Salmonella typhimurium,* which causes salmonellosis. On binding to the DNA target, nanoparticles approach each other, which results in UCNP photoluminescence quenching; this allows quantitative determination of the target DNA.[69] Wang and Li[120] used magnetic nanoparticles instead of gold nanoparticles. This method is based on quantitative determination of the target DNA from the level of photoluminescence of the self-assembled structures containing UCNPs and magnetic particles, which are withdrawn from the solution under the action of magnetic field.[120]

VII.2. Antigen – antibody

An antigen – antibody system of molecular adaptors was used for visualization of the Ki-67 cell proliferation biomarker in human cervical carcinoma HeLa cells. For this purpose, ZrO_2 : Yb,Er UCNPs were coated with the biotinylated mouse anti-rabbit antibody and then with rabbit anti-Ki-67 antibody.[24]

VII.3. (Strept)avidin – biotin

The (strept)avidin – biotin is the most demanded and traditionally widely used system. Avidin, a glycoprotein from egg white, and its functional analogue, streptavidin, produced by the bacteria *Streptomyces avidinii*, possess exceptionally high affinity for biotin (vitamin H). A distinctive feature of the formed complexes is the stability against harsh environment, including temperature [the melting point of the (strept)avidin – biotin complex is 112 °C] and pH variations, as well as the action of enzymes and denaturing agents.[121]

The self-assembly was modelled using biotinylated UCNPs and avidin conjugated with the fluorescein isothiocyanate (FITC) fluorochrome. After the self-assembly of bioconjugates in the solution, a FITC signal was measured, which was 25 times as intense as the signal obtained after physisorption of avidin – FITC conjugates on non-biotinylated UCNPs.[20] The limit of detection of avidin sorbed in the plate wells using photoluminescence contrasting with biotinylated UCNPs was 1.8 μmol, which is sufficient for implementation of this system as an analytical biochemistry technique.[25] The avidin detection in a solution can be based on the UCNP photoluminescence quenching *via* resonance energy transfer. It was shown that even traces of avidin present in a colloid solution of biotinylated UCNPs and biotinylated gold nanoparticles decrease the level of UCNP photoluminescence in proportion to the amount of avidin.[66]

A two-stage procedure for highly sensitive determination of the level of protein kinase expression *in vitro* was developed on the basis of UCNPs and the avidin – biotin pair. This level often serves as an important criterion for planning the therapy of cancer and Alzheimer's disease. The procedure is based on the use of a biotinylated peptide substrate, which is phosphorylated in the presence of protein kinases and ATP. Then the phosphorylated peptide is collected from the solution by Zr^{4+}-functionalized magnetic beads *via* Zr^{4+} binding to the phosphate group and treated with UCNP – avidin bioconjugates for quantitative determination.[62] In another study, UCNP – streptavidin bioconjugates were proposed for evaluation of the activity of the endonuclease benzonase, which cleaves oligonucleotides into smaller fragments. For this purpose, the nucleotide substrate conjugated with the Alexa Fluor 680 fluorochrome and biotin on one end and fluorescence quencher on the other end was treated with the enzyme. The released biotinylated fragments were bound to UCNP – streptavidin bioconjugates and quantified on the basis of fluorescence of Alexa Fluor 680, which received excitation energy from UCNPs on exposure to near-IR radiation (see description of the Förster resonance energy transfer below, in Section IX).[122]

The UCNP – streptavidin bioconjugates were also linked to biotinylated antibodies,[54] including the antibody against the prostate specific antigen located on cell surfaces[81] or histological sections of human prostate tissue;[19] to a biotinylated aptamer with affinity for nucleolin or prion on the human hepatoma cell surface;[64] and to DNA molecules.[69]

However, despite the benefits of the (strept)avidin – biotin system as a molecular adaptor, the preparation of target assemblies involving this system is still a labour-consuming task. Furthermore, noticeable quantities of biotin are present in the blood and tissues of mammals and can competitively bind to (strept)avidin incorporated in the self-assembled units upon systemic administration into the body, and the tetrameric structure of (strept)avidin increases the probability of aggregation of biotinylated UCNPs.

VII.4. Barnase – barstar

The bacterial ribonuclease barnase (Bn) and its natural inhibitor barstar (Bs) form a strong complex with a very low dissociation constant [only an order magnitude

higher than that of the (strept)avidin–biotin constant].[123] The Bn–Bs system is distinguished among other functional analogues by a number of advantages. They include easy production in biotechnological expression systems (including bacterial ones), low level of immunogenicity due to relatively small size, and high stability to elevated temperature (up to 50 °C), to the action of denaturing agents[124] and to pH variation (in the range from 2 to 12).[125] These proteins are monomers with their ends free for fusion and bioconjugation.[126–130] For example, the fusion protein of Bn and the scFv fragment of the 4D5 anti-HER2/neu antibody was attached to the UCNP–Bs bioconjugate for visualization of the human breast adenocarcinoma SK-BR-3 cells.[75] Barstar was attached to the surface carboxyl groups of UCNP–PMAO using 3-(3-dimethylaminopropyl)-1-ethylcarbodiimide hydrochloride and *N*-hydroxysulfosuccinimide as cross-linking agents. High binding selectivity to tumour cells was demonstrated for this two-component assembly by two-stage delivery. First, the cells were treated with the 4D5scFv–Bn module for recognition, ad then the UCNP–Bs contrast module was added; the latter was attached to the 4D5scFv–Bn module already immobilized on the HER2/neu tumour marker and thus provided visualization.

Thus, using molecular adaptors, it is possible to obtain a variety of hybrid assemblies based on UCNPs by mere mixing of the required modules loaded with adaptor molecules and to perform preliminary targeting on a particular site or quantitative determination of the DNA content and enzyme activity.

VIII. Biocompatibility of upconversion nanoparticles

VIII.1. Cytotoxicity

The upconversion nanoparticles are attracting increasing attention in various fields of biomedicine as promising photoluminescent materials. However, to introduce methods based on the use of UCNPs into research and clinical practice, it is necessary to study the effects caused by accumulation of the particles in cells and tissues, their cytotoxicity and patterns of biodistribution in a living body and excretion from the body. As opposed to well-known quantum dots, UCNPs do not contain elements of toxicity classes I or II such as cadmium or selenium.[5] The photoluminescence of UCNPs is caused by lanthanide ions, the median lethal dose of which is, most often, an order of magnitude higher.[131]

According to the publications devoted to the biocompatibility of UCNPs, various types of UCNPs show rather high biocompatibility levels irrespective of the surface modification.[2] However, since the $NaYF_4$:Yb,Er UCNPs are used most widely, the cytotoxicity of particularly this material arouses enhanced interest. Three types of cytotoxicity mechanisms were proposed for UCNPs with the $NaYF_4$ matrix, in particular, oxidative stress, release of Y^{3+} ions, which influence cell functions, and release of surface modification agents in the acid medium of lysosomes.[132] In addition, potential UCNP cytotoxicity may be caused by the presence of oleic acid molecules on the nanoparticle surface. It was shown that after partial removal of oleic acid on treatment with tetramethylammonium hydroxide, UCNPs possess moderate cytotoxicity towards keratinocytes, the viability of which decreases to 76% ± 3% after incubation for 24 h.[73]

The degree of toxic action of UCNPs with different types of surface modification in various concentrations and for various exposure times has now been studied. Most of the studies dealing with evaluation of cytotoxicity of UCNPs, first of all, UCNP-SiO_2, were performed on cell cultures *in vitro*. It was shown that UCNP($NaYF_4$:Yb,Er)-SiO_2 in concentrations of < 1 mg ml^{-1} have no significant effect on the viability of human cervical carcinoma HeLa cells irrespective of the incubation time.[133] However, moderate cytotoxicity (decrease in the cell viability by ~30% in 48 h) was found for UCNP-SiO_2 in 100 mg ml^{-1} concentration towards rat skeletal myoblasts, rat bone marrow mesenchymal stem cells[68] and human breast cancer MCF-7 cells.[93] The presence of functional groups on the UCNP surface can substantially change the situation. For example, modification of the SiO_2 coating *via* carboxylation, amination or PEGylation had different effects on the UCNP-SiO_2 biocompatibility. Aminated UCNP-SiO_2 were most toxic, while carboxylated ones were least toxic. This finding was attributed to the fact that the cell membrane has a negative potential and attracts positively charged particles; this induces their enhanced endocytosis and, consequently, higher toxicity. In addition, in the cultural medium, particles are coated with a layer of proteins with a density depending on the charge. The least density and most bulk of the shell are observed on the surface of non-charged UCNP-PEG particles, which prevents them from penetration into the cells but induces strong immune response from living cells.[132] The proliferative activity of human cervical carcinoma HeLa cells decreased by 50% upon incubation with UCNP-SiO_2-NH_2 in a concentration of ~500 μg ml^{-1} for 3 days.[133]

A similar dependence was observed upon surface modification of UCNPs with organic polymers containing amino and carboxyl groups. The viability of human cervical carcinoma HeLa cells decreased to < 60% in 24 h under the action of UCNP($KGdF_4$:Yb,Er)-PEI in a concentration of 5 mg ml^{-1}; meanwhile, upon exposure to UCNPs modified with 6-aminocaproic acid in the same concentration, > 80% of the cells survived.[33]

As noted above, different types of cells react in different ways to the action of UCNPs. This was considered by Guller *et al.*[73] in relation to the effect of $NaYF_4$:Yb,Er UCNPs with different types of surface modification on the healthy cells of human skin, including fibroblasts and HaCaT keratinocytes. The incubation of fibroblasts for 24 h in the presence of UCNPs (in concentrations of 62.5 and 125 μg ml^{-1}) coated with PEI, dextran sulfate, poly(D,L-lactide), poly(lactide-*co*-glycolide) (PLG), PMAO or encapsulated into polystyrene microspheres, in particular, together with magnetic Fe_2O_3 nanoparticles, did not have a statistically significant influence on the cell viability. Meanwhile, the viability of keratinocytes varied depending on the type of the coating (Fig. 13). The highest cytotoxicity was detected in the case of PEI (52% ± 4%), PLG (61% ± 2%) and dextran sulfate (72% ± 8%); this was not correlated with the level of internalization into cells, which varied from 1.8% to 46%. At medium levels of internalization of UCNP-poly(D,L-lactide) (59%) and

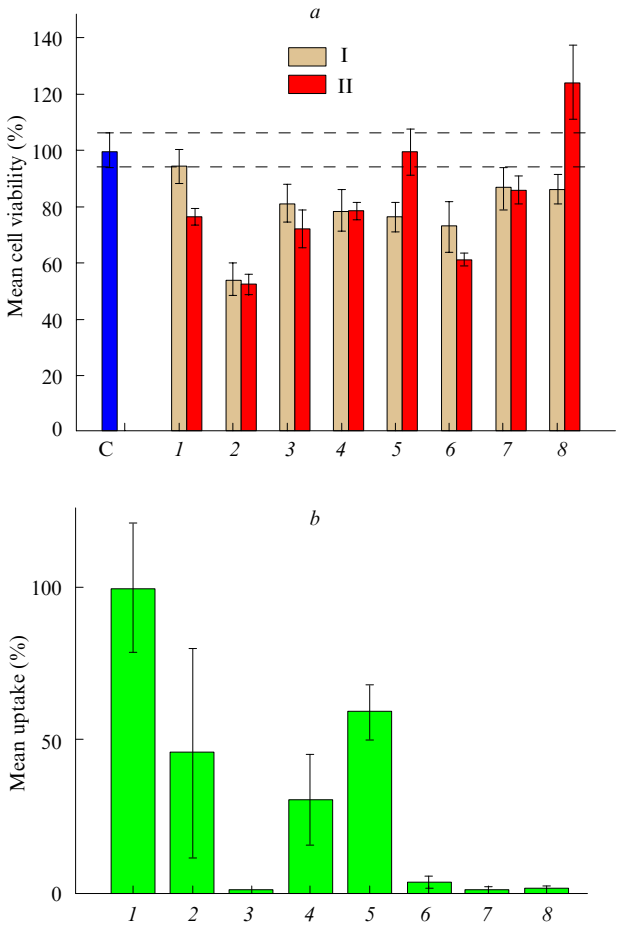


Figure 13. Effect of surface modification of UCNPs on the viability characteristics of human epithelial HaCaT keratinocytes (I, mean cell viability after incubation with UCNPs in a concentration of 62.5 μg ml^{-1}; II, 125 μg ml^{-1}) (*a*) and on cellular uptake by HaCaT keratinocytes (*b*).[73]
C is control, (*1*) UCNPs, (*2*) UCNP-PEI, (*3*) UCNP-dextran sulfate, (*4*) UCNP-PMAO, (*5*) UCNP-poly(D,L-lactide), (*6*) UCNP-PLG, (*7*) polystyrene – UCNP, (*8*) polystyrene – (UCNP + Fe_2O_3).

UCNP-PMAO (30%), their effect on the viability of the cells was insignificant.[73] The polystyrene microspheress with UCNP and Fe_2O_3 inclusions did not have a marked cytotoxic effect either; however, the large size of the microspheres (> 200 nm) prevented them from cellular uptake. Enhancement of the cell growth with increasing concentration of polystyrene microspheres was attributed to the formation of scaffolds for attachment upon the aggregation of microspheres.

The highest biocompatibility is imparted to UCNP by natural materials. Encapsulation of oleylamine-coated $NaYF_4$:Yb,Er UCNPs into an albumin shell reduced the cytotoxicity 10-fold.[83] Low cytotoxicity of UCNP modified with a chitosan derivative, in a concentration of 200 μg ml^{-1} was demonstrated for incubation with human cervical carcinoma HeLa cells: after 24 h, the cell viability was ~85%.[37] Yuan *et al.*[53] achieved biocompatibility by encapsulating UCNPs into a DNA shell *via* electrostatic interaction of negatively charged DNA molecules with positively charged thiol groups introduced on the UCNP-SiO_2-Ag surface. Within 24 h, the viability of B16F0 cells incubated with UCNP-DNA in a concentration of 400 μg ml^{-1} decreased by 8%.[53]

The attachment of targeted delivery agents often increases the biocompatibility of UCNPs. For example, the survival percentage of the human breast cancer MCF-7 cells and mouse embryonic fibroblasts 3T3 after a 24-h incubation with UCNP – immunoglobulin bioconjugates in a concentration of 100 μg ml^{-1} was more than 90%.[134] After 24-h exposure of human cervical carcinoma HeLa cells with UCNP – FA bioconjugates in a concentration of 1000 μg ml^{-1}, the viability of cells was ~90%.[55, 112]

VIII.2. General toxicity

Some papers deal with the general toxicity of UCNPs at the organism level, including the effects on the structure and functional state of cells and tissues and biodistribution of surface-modified UCNPs in the normal and pathological animal organs.

According to the published results, UCNPs have good biocompatibility *in vivo* provided that surface modification has been performed and hydrophilicity has been ensured. The conclusions about good biocompatibility of UCNPs are based on the results of numerous studies involving intravenous injection of UCNPs into laboratory animals (rats, mice and chicken and fish embryos). A week after laboratory mice were intravenously injected with UCNPs coated with polyhedral oligomeric silsesquioxane, no pulmonary fibrosis, necroses, or inflammatory or degenerative processes in myocardial cells and hepatocytes were detected; the kidney glomerular structure was not disturbed; and no inflammatory reactions were present.[77] Monitoring of the animal body weight carried out for 115 days after administration of UCNP($NaYF_4$:Yb,Tm)-PAA did not show any adverse effects on the health of test mice.[63] In a study of the effect of UCNP(LaF_3:Yb,Er)-SiO_2-NH_2 on the *Danio rerio* fish embryo development, an adverse effect on the embryo was found only for high concentrations of these particles. The introduction of 10 nl of UCNP-SiO_2-NH_2 in a concentration of > 200 μg ml^{-1} into deutoplasm caused genetic damages, probably, due to binding of lanthanide ions to DNA molecules.[27]

VIII.3. Biodistribution

The biodistribution of UCNPs with different types of surface modification in the body was studied in several works considering intravenous injection of UCNPs in test animals. The UCNPs coated with azelaic acid were shown to freely circulate in the blood stream of mice without aggregation.[89] Furthermore, in the case of injection of differently charged particles, UCNP-SiO_2-NH_2, UCNP-SiO_2-CO_2H and UCNP-SiO_2-PEG, in chicken embryos, the UCNP circulation time does not depend on the nature of the modifying agent, being 20 – 25 min in all cases.[135] However, the UCNP excretion rate depends on the particle size: UCNP-PAA of ~10 nm size were rapidly excreted from the mouse body, whereas larger particles were mainly accumulated in the liver and spleen and were excreted very slowly.[63]

According to different data, the UCNPs injected in the mouse tail vein are mainly accumulated in the liver

and spleen, as was shown for UCNPs coated with azelaic acid,[89] and in lungs (for UCNP coated with polyhedral oligomeric silsesquioxane),[77] intestines and kidneys [for UCNP-chitosan-FA (chitosan-FA is chitosan modified with folic acid residues)].[82] The main bulk of UCNP-SiO_2 intravenously injected in Wistar rats were concentrated in the lungs and heart.[68] Chatterjee *et al.*[84] studied the distribution of UCNP-PEI in rat organs using inductively coupled plasma mass spectrometry by determining the content of Y^{3+} ions at specified time intervals after injection into the blood stream. The peak concentration of UCNPs was observed immediately after the injection in lungs and after 24 h in spleen. On the 7th day, only trace amounts of UCNPs were found in the organs of test animals.[68, 84, 85]

IX. Therapeutic applications of upconversion nanoparticles

Several recent publications are devoted to therapeutic applications of UCNPs. They mainly focus on the development of methods for photodynamic therapy.[136] Some publications describe the use of UCNPs for delivery and controlled release of drugs[109] and genetic material.[137]

IX.1. Targeted drug delivery

The delivery of therapeutic agents to target lesions was demonstrated for the chemotherapetic agent doxorubicin. Its cytotoxic effect is caused by a number of factors, including intercalation between the G···C base pairs in DNA, which disrupts replication and transcription and the binding of DNA-synthesis enzymes and other biologically significant molecules. However, the use of free doxorubicin gives rise to numerous adverse effects during the therapy such as hematopoiesis disorder. The use of UCNP platform for the transfer of doxorubicin sorbed on the surface allows selective release of the agent in cancer cells owing to low pH ($\leqslant$6.15) inherent in these cells, as was shown for the human breast cancer MCF-7[32] and human nasopharyngeal epidermoid carcinoma KB[109] cell lines. The doxorubicin desorption over a period of 24 h increases from 12% at pH 7.4 to 30% at pH 6.[31]

It was found in mouse experiments that immobilization of doxorubicin molecules on the UCNP surface increases the retention time in the blood stream compared with the molecular form of the agent and causes a 1.7-fold increase in the therapeutic effect towards the mouse hepatoma H22 allografts.[31]

IX.2. Photosensitizing assemblies based on upconversion nanoparticles

Photodynamic therapy is a method for treatment of cancer and infectious diseases based on the use of light-sensitive compounds called photosensitizers. Photosensitizers are delivered to the lesions and irradiated at a wavelength that falls in their optical absorption region in the presence of oxygen; this induces a photochemical reaction, which affords singlet oxygen and highly reactive radicals. Singlet oxygen and radicals induce necrosis and apoptosis of adjacent tissues.

Most of known photosensitizers are porphyrin and phthalocyanine derivatives with intense light absorption in the UV and visible spectral regions. However, excitation of a photosensitizer in the visible region may bring about photodestruction of healthy tissues and the fluorescence response of tumour cells, which affects the efficiency of formation of singlet oxygen.[49] Some photosensitizers are hydrophobic and toxic in the free state.[136] For solving these issues, Zhang *et al.*[138] proposed using the Förster energy transfer — non-radiative energy transfer between the donor and the acceptor, resulting in quenching of photoluminescence of the donor (in this case, UCNPs) and in longer-wavelength fluorescence of the acceptor (photosensitizer). The use of UCNPs as donors has a number of benefits. First, the large spectral gap between the absorption range of UCNPs and most photosensitizers rules out direct excitation of the latter. Second, the narrow UCNP emission spectra minimize their overlap with the photosensitizer emission range; this enables reliable control over the energy transfer from the donor to the acceptor. Third, the use of UCNPs with a hydrophilic shell obviates the need for chemical modification of the photosensitizer.[2] Fourth, the near-IR excitation increases the depth of penetration into the living tissue with insignificant autofluorescence.[82]

The methods used to attach photosensitizers to UCNPs include simple sorption, incorporation into the shell and covalent or hydrophobic binding. Each strategy has its own advantages and drawbacks. Physisorption is inferior to other methods as the attachment is reversible, and the drawback of covalent binding is a limited number of sites.[82] The photosensitizer attachment techniques based on the interaction with hydrophobic surface groups or incorporation into the shell decrease the energy transfer efficiency.[111]

IX.2.a. Covalent binding

Examples of covalent conjugates reported in the literature include UCNPs linked to the photosensitizers Rose Bengal *via* 2-aminoethyl dihydrogen phosphate[58] and chlorin e6 (Ce6) *via* the amino groups on the SiO_2 shell.[139] Often, the SiO_2 shell is made porous in order to increase the surface of binding and to protect the photosensitizer against photooxidation. For example, hematoporphyrin and silicon phthalocyanine dihydroxide were covalently grafted to mesoporous SiO_2 shell of UCNPs.[49]

IX.2.b. Physisorption

The direct physisorption, which allows the maximum proximity of the photosensitizer molecules and UCNPs, is used to achieve the best efficiency of energy transfer and increase in the amount of $^1O_2$ formed. The efficiency increases to 96.3% when the $LiYF_4$:Yb,Er UCNP is used as the donor and Zn phthalocyanine (Pc) serves as the acceptor.[43] The sorption is performed on the UCNP surface deprived from oleic acid molecules by acid or ultrasonic treatment. To avoid aggregation, the UCNP surface is additionally modified with a polymer shell to prevent the interaction of photosensitizer molecules.[43] Direct attachment of a fullerene C_{60} derivative as a photosensitizer to UCNPs was carried out using the oleylamine displacement strategy.[111] Indirect sorption implies the presence of an intermediate layer between the UCNP and the sensitizer, as, for example, in UCNP-PEI-Pc.[61, 140]

IX.2.c. Incorporation in the shell

The incorporation in the shell is used to fabricate structures with high content of a photosensitizer protected from the environment. The photosensitizer can be incorporated both during UCNP preparation to surface modification and after the shell has been formed. For example, Ce6 was conjugated with polyelectrolytes, which were then loaded onto UCNP;[67] merocyanine-540 (MC540) was introduced into a SiO_2 shell during polycondensation on the UCNP surface;[138] Pc was incorporated into the already formed mesoporous SiO_2 shell.[141] However, hydrophobic binding is used most often to incorporate photosensitizers into the shell. Binding occurs with oleic acid (for *meso*-tetraphenylporphin, MC540 and Ce6 photosensitizers),[42, 136, 142] PMAO (Ce6),[143] phospholipid (Ce6)[85] or chitosan (Pc)[82] shells. In most cases, the particles are then encapsulated into an additional polymer in order to protect the sensitive hydrophobic interactions from pH fluctuations.[82]

IX.3. Targeted delivery of photosensitizing assemblies based on upconversion nanoparticles

The accumulation of UCNP-based photosensitizing assemblies in a tumour can be enhanced by using hydrophobic photosensitizers, pH-dependent agents or targeted delivery agents.

The incorporation of hydrophobic Ce6 molecules into the phospholipid shell promoted better accumulation of UCNPs in the mouse xenograft models of human glioblastoma U87MG (Fig. 14).[85]

The surface modification of UCNPs by a pH-dependent polymer based on dimethylmaleic acid (DMMA) and PEG, which switches negative charge to positive one as pH decreases to 6.8, improved the interaction with negatively charged tumour cells in which pH varied in the 6.5 – 6.8 range. Upon the intravenous injection of UCNP-Ce6-PEG-DMMA into Balb/c inbred mice with breast cancer 4T1 xenografts, accumulation in the tumour increased 6.4-fold as compared with the negatively charged particles.[67]

According to published data, the first UCNP-based photosensitizing assemblies for targeted delivery were covalent conjugates of UCNP-SiO_2 with inclusions of the MC-540 photosensitizer and the monoclonal anti-MUC1/episialin antibody (anti-MUC1/episialin is the tumour marker expressed on the human breast cancer MCF-7/AZ cell surface).[138] More recently, other systems, most often containing FA as the target delivery agent such as UCNP-Pc,[61] UCNP-Rose Bengal,[58] UCNP-C_{60}[111] and UCNP-MC540,Pc[92] have been developed. The UCNP-MC540,Pc-FA system was used to demonstrate the targeted delivery *in vivo* in a mouse body with B16-F0 melanoma. The combined action of the MC540 and Pc photosensitizers resulted in a considerable increase in the therapeutic effect as compared with the systems containing only one of these photosensitizers.[92]

IX.4. Therapeutic efficiency of photosensitizing assemblies based on upconversion nanoparticles

Most of UCNP-based photosensitizing assemblies demonstrate high antitumour activities both *in vitro* and *in vivo* on model animals. For example, incubation of human cervical carcinoma HeLa cells with 250 ng litre^{-1} of UCNP-*meso*-tetraphenylporphin for 48 h and the subsequent irradiation resulted in the death of 75% of cells.[136] The UCNP-Ce6 photosensitizing assemblies were among the first to be used in experiments with animals; they demonstrated exceptionally high efficiency towards breast cancer 4T1 xenografts implanted in Balb/c inbred mice. Within 60 days after the intratumoral injection of UCNP-Ce6 followed by a 15-min irradiation with a laser at 980 nm, complete degradation of the tumour was observed in 7 cases out of 10; furthermore, UCNP-Ce6 were excreted from the body almost completely as soon as 2 weeks after administration without any visible health impacts in the test animals. A noticeable therapeutic effect could be achieved even when the xenografts

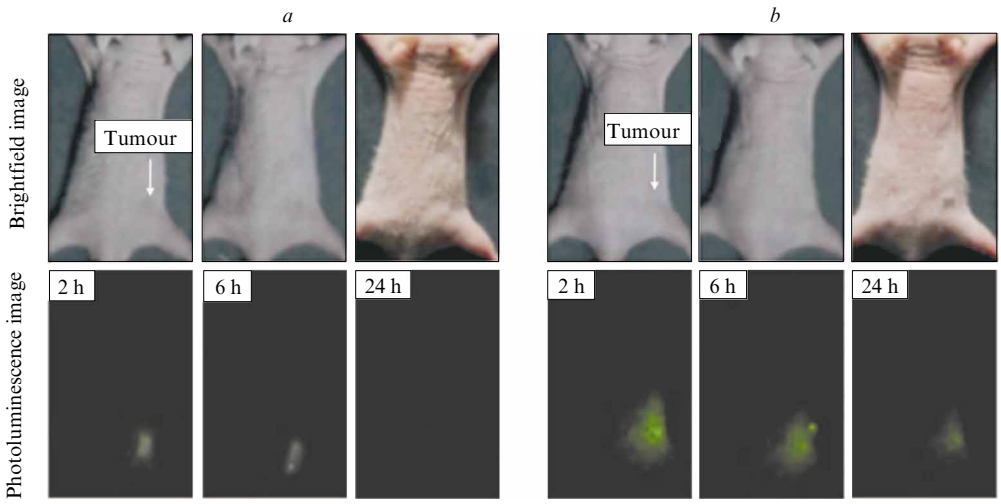


Figure 14. Photoluminescence images of the U87MG mouse xenografts recorded 2, 6 and 24 h after intravenous injection of UCNPs (*a*) and UCNP-Ce6 (*b*) and corresponding brightfield images of the injected mice.[85]

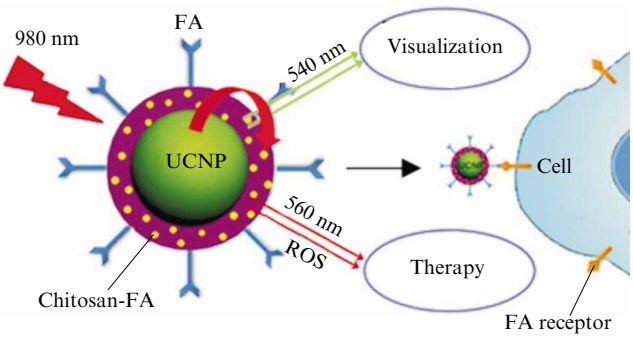


Figure 15. Illustration of the principle of action of the UCNP-Pc-FA photosensitizing assembly on the cancer cells overexpressing the FA receptor.[82]
ROS are reactive oxygen species.

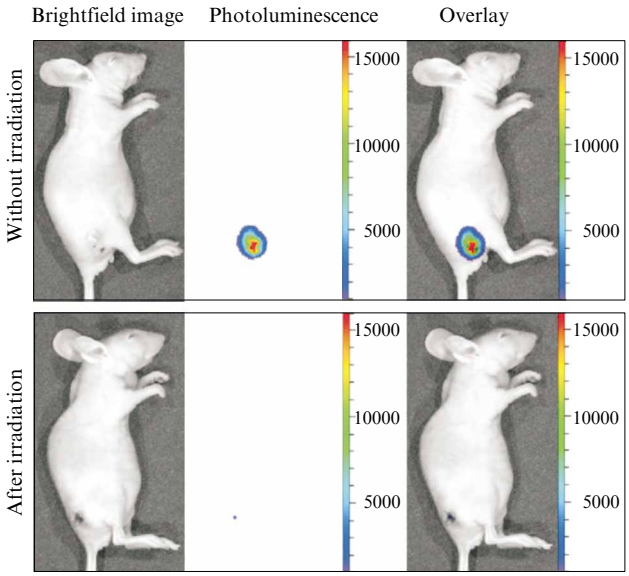


Figure 17. Degradation of the human cervical carcinoma Hela-*luc* xenograft in the Balb/c inbred mouse body two weeks after the phototoxic action.[144]

were irradiated through a 8 mm thick pork tissue slice.[143] The attachment of Ce6 increases the UCNP lifetime in the blood stream 5-fold, apparently, owing to the enhanced colloid stability, but it considerably reduces the red (660 nm) emission from UCNP as a result of efficient energy transfer.[85]

The therapeutic efficiency of targeted UCNP-Pc-FA bioconjugates against the mouse sarcoma S180, expressing the FA receptor, was 66%, while with irradiation through 1 cm-thick porcine adipose tissue, it was 50%.[82] The schematic view of the UCNP-Pc-FA photosensitizing assembly is shown in Fig. 15 together with the illustration of the photodynamic therapy mechanism accompanied by the optical monitoring of the therapeutic action.

A fairly high therapeutic efficiency was achieved when the UCNP-MC540 assemblies were enclosed into erythrocyte vesicles and decorated with molecules of lipophilic derivatives of FA and the mitochondrial triphenylphosphonium shuttle cations. The assemblies were fabricated by extruding the components through a membrane. An erythrocyte membrane served to protect the UCNP-MC540 system from entrapment with the immune and reticulo-endothelial system cells and to perform the intracellular transport of the vesicle content by fusion with the target cell membrane. Owing to the well-established oxygen transport mechanism, the erythrocyte membrane also promoted the transfer of triplet oxygen to the photo-

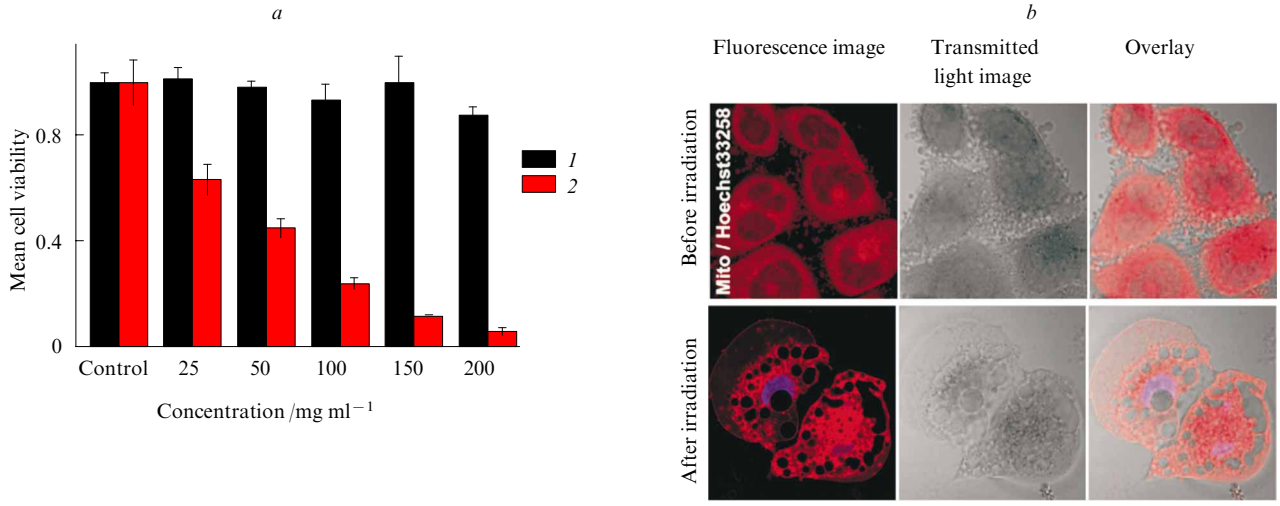


Figure 16. Antitumour activity of the UCNP-PC_{70}-FA photosensitizing assembly.[144]
(*a*) Results of colorimetric MTT test on the determination of Hela-*luc* cell viability obtained after 24 h of incubation with UCNP-PC_{70}-FA in various concentrations in the dark (*1*) and after irradiation with a laser at 980 nm (*2*); (*b*) confocal images of the cells contrasted with MitoRed (mitochondria) and Hoechst 33258 (nuclei) before and after the phototoxic action and corresponding cell images in the transmitted light.

sensitizer and the release of short-lived (several milliseconds) singlet oxygen in the target lesion. In *in vitro* experiments with the human melanoma B16 cell culture, it was shown that after penetration into the cell, 95% of UCNP-MC540 is sequestrated in lysosomes, which substantially reduces the therapeutic effect. Encapsulation into an erythrocyte membrane and decoration with FA and triphenylphosphonium ensured targeted delivery of ~92% of the assemblies to the cell mitochondria where the impact of singlet oxygen is most detrimental. In *in vivo* experiments on mice, the therapeutic effect correspondingly increased. Encapsulation into an erythrocyte membrane with dual targeting function enhanced the antitumour effect against the human melanoma B16 xenografts by an order of magnitude; this was due to the 2.3-fold increase in the volume of blood-circulating UCNPs and enhancement of the targeting function.[142]

The porphyrin – fullerene dyad PC_{70}, which has a relatively long triplet state lifetime, was proposed as the photosensitizer to achieve the best effect under oxygen deficiency inherent in the tumour tissue.[144] The PC_{70} dyad was sorbed on the surface of citric acid-modified UCNPs with subsequent bioconjugation with FA for targeted delivery to human cervical carcinoma Hela-*luc* cells. The mean cell viability of Hela-*luc* cells *in vitro* markedly decreased with increasing the concentration of the UCNP-PC_{70}-FA used (Fig. 16 *a*). The degradation of irradiated cells contrasted by the fluorescent dyes MitoRed (mitochondria) and Hoechst 33258 (nuclei) was imaged by confocal microscopy (see Fig. 16 *b*).

The maximum efficiency of tumour damage *in vivo* was achieved by laser irradiation of mouse xenograft models at 980 nm after intravenous injection of 400 μg of UCNP-PC70-FA. Figure 17 illustrates the noticeable regression of the xenografts irradiated at the time instant of maximum accumulation of UCNP-PC70-FA (24 h after the administration).[144]

IX.5. Biocompatibility of photosensitizing assemblies based on upconversion nanoparticles

Low degrees of dark cytotoxicity were established for most UCNP-based photosensitizing assemblies, including UCNP-Rose Bengal-FA (no cytotoxicity at a concentration of 150 μg ml^{-1}),[58] UCNP-PC (5% cell death at a concentration of 1 mg ml^{-1}),[43] UCNP-*meso*-tetraphenylporphin (no cytotoxicity at a concentration of 14.9 μg ml^{-1}),[136] UCNP-MC540 encapsulated into an erythrocyte membrane with dual targeting (3.3% cell death at a concentration of 25 μg ml^{-1}).[142] The half-maximal cytotoxicity of UCNP-Ce6 in the dark was achieved by the incubation of human breast cancer MCF-7 cell line with UCNP-Ce6 in a concentration of 400 μg ml^{-1} for 24 h.[139]

The histological analysis of heart, lung, kidney, liver and spleen tissues of test animals did not reveal any pathology related to the use of UCNP-C_{60}-FA bioconjugates.[111]

IX.6. Combined therapy

The use of inorganic UCNP platform for the assembly of therapeutic structures makes it possible to combine several therapeutic components in one system to achieve a combined effect and, simultaneously, to monitor the results. For example, for affecting a cancer tumour, the photosensitizing assemblies UCNP-Ce6 were loaded with the genetic therapy agent siRNA suppressing the expression of the Plk1 oncogen through sorption on the external PEI layer.[42] In another study aimed at the development of an antitumour agent with joint action, UCNPs were coated with a layer of an amphiphilic photosensitizer linked to doxorubicin *via* an *o*-nitrobenzyl bridge, which is cleaved on exposure to UV radiation. The photoluminescence of UCNPs initiated the formation of singlet oxygen with participation of the photosensitizer molecules and release of the chemotherapeutic agent doxorubicin as a result of bridge cleavage. The tripeptide RGD was covalently attached to an assembly targeting human glioblastoma U87MG cells with overexpression of the $\alpha_v\beta_3$ integrin receptor. The half-maximal effect of the use of conjugates was doubled by the introduction of doxorubicin and was achieved at a concentration as low as 14.6 μg ml^{-1}.[113]

IX.7. Anti-infective agents

Apart from the therapy of cancer, an equally promising application area of the UCNP-based photosensitizing agents is the therapy of infectious diseases. For example, the UCNP-Pc system loaded with the anti-Dengue virus envelope protein antibody was shown to induce the photodynamic degradation of the virus in the human hepatoma HepG2 cells *via* oxidation of guanosine residues, phospholipids and virus envelope proteins.[140] The UCNP-based photosensitizing assemblies containing curcumin (plant polyphenol) were successfully used to treat the pulmonary methicillin-resistant staphylococcal infection in mice by intravenous administration.[145]

X. Conclusion

Unpconversion nanoparticles represent a relatively new class of inorganic nanoparticles possessing a great potential for various applications in biomedical research, ranging from imaging of biological targets at the molecular level to the therapy of cancer and infectious diseases. The unique physicochemical properties of UCNPs including the programmed spectra and narrow photoluminescence peaks, excitation in the near-IR range, large two-photon absorption cross-sections and stability to photobleaching can be used to considerably extend the scope of modern optical methods used in biomedical practice. The application of UCNPs makes it possible to solve problems that are difficult to address using the conventional fluorochromes: simultaneous detection of several biological targets, monitoring of molecular processes on a real-time basis for long periods of time and imaging of lesions deep in the tissues. Owing to a relatively large UCNP surface area accessible for chemical modification, it is possible to attach molecules capable of targeted delivery, therapeutic action and so on. Thus, the agent delivery to the target lesion can be combined with monitoring of this process. Further design of UCNP-based diagnostic and therapeutic agents would promote the development of innovative approaches in oncology, including image-guided surgery, determination of the molecular profile of cancer tumours, personalized diagnosis and therapy. The success of implementation of the huge UCNP potential and extensive use of UCNPs in the clinical and analytical practice will depend on the solution of relevant

tasks related to optimization of optical detection conditions and on the research aimed at increasing biocompatibility and upconversion efficiency.

This review was prepared with the support from the Russian Science Foundation (Project No. 14-24-00106).

References

1. F Auzel *Chem. Rev*. **104** 139 (2004)
2. C Bouzigues, T Gacoin, A Alexandrou *ACS Nano* **5** 8488 (2011)
3. S Wu, G Han, D J Milliron, S Aloni, V Altoe, D V Talapin, B E Cohen, P J Schuck *Proc. Natl. Acad. Sci. USA* **106** 10917 (2009)
4. M Yu, F Li, Z Chen, H Hu, C Zhan, H Yang, C Huang *Anal. Chem*. **81** 930 (2009)
5. L Zhao, A Kutikov, J Shen, C Duan, J Song, G Han *Theranostics* **3** 249 (2013)
6. L-D Sun, H Dong, P-Z Zhang, C-H Yan *Annu. Rev. Phys. Chem*. **66** 619 (2015)
7. P Qiu, N Zhou, H Chen, C Zhang, G Gao, D Cui *Nanoscale* **5** 11512 (2013)
8. J Chen, J X Zhao *Sensors* **12** 2414 (2012)
9. X Li, D Zhao, F Zhang *Theranostics* **3** 292 (2013)
10. L Wei, S Doughan, Y Han, M V DaCosta, U J Krull, D Ho *Sensors* **14** 16829 (2014)
11. Y Min, J Li, F Liu, P Padmanabhan, E K L Yeow, B Xing *Nanomaterials* **4** 129 (2014)
12. C Wang, L Cheng, Z Liu *Theranostics* **3** 317 (2013)
13. C T Xu, Q Zhan, H Liu, G Somesfalean, J Qian, S He, S Andersson-Engels *Laser Photonics Rev*. **7** 663 (2013)
14. L Cheng, C Wang, Z Liu *Nanoscale* **5** 23 (2013)
15. G Han, G Chen *Theranostics* **3** 354 (2013)
16. G Chen, G Han *Theranostics* **3** 289 (2013)
17. S Jiang, K Y Win, S Liu, C P Teng, Y Zheng, M-Y Han *Nanoscale* **5** 3127 (2013)
18. T Soukka, K Kuningas, T Rantanen, V Haaslahti, T Lövgren *J. Fluoresc*. **15** 513 (2005)
19. H J M A A Zijlmans, J Bonnet, J Burton, K Kardos, T Vail, R S Niedbala, H J Tanke *Anal. Biochem*. **267** 30 (1999)
20. S Sivakumar, P R Diamente, F C J M van Veggel *Chem. – Eur. J*. **12** 5878 (2006)
21. J Zhao, Z Lu, Y Yin, C McRae, J A Piper, J M Dawes, D Jin, E M Goldys *Nanoscale* **5** 944 (2013)
22. R H Page, K I Schaffers, P A Waide, J B Tassano, S A Payne, W F Krupke, W K Bischel *J. Opt. Soc. Am. B* **15** 996 (1998)
23. C Vinegoni, D Razansky, S A Hilderbrand, F Shao, V Ntziachristos, R Weissleder *Opt. Lett*. **34** 2566 (2009)
24. A Ceja-Fdez, T López-Luke, J Oliva, J Vivero-Escoto, A L Gonzalez-Yebra, R A R Rojas, A Martínez-Pérez, E de la Rosa *J. Biomed. Opt*. **20** 046006 (2015)
25. Y Ai, D Tu, W Zheng, Y Liu, J Kong, P Hu, Z Chen, M Huang, X Chen *Nanoscale* **5** 6430 (2013)
26. T Zako, H Nagata, N Terada, M Sakono, K Soga, M Maeda *J. Mater. Sci*. **43** 5325 (2008)
27. K Wang, J Ma, M He, G Gao, H Xu, J Sang, Y Wang, B Zhao, D Cui *Theranostics* **3** 258 (2013)
28. V Nguyen, T K C Tran, D V Nguyen *Adv. Nat. Sci.: Nanosci. Nanotechnol*. **2** 045011 (2011)
29. Q Lm, F Guo, L Sun, A Li, L Zhao *J. Appl. Phys*. **103** 123533 (2008)
30. T Konishi, K Shimizu, Y Saito, K Soga *J. Photopolym. Sci. Technol*. **20** 11 (2007)
31. Y Chen, B Liu, X Deng, S Huang, Z Hou, C Li, J Lin *Nanoscale* **7** 8574 (2015)
32. S Huang, Z Cheng, Y Chen, B Liu, X Deng, P Ma, J Lin *RSC Adv*. **5** 41985 (2015)
33. H-T Wong, M-K Tsang, C-F Chan, K-L Wong, B Fei, J Hao *Nanoscale* **5** 3465 (2013)
34. H-X Mai, Y-W Zhang, L-D Sun, C-H Yan *J. Phys. Chem. C* **111** 13721 (2007)
35. Z Song, Y G Anissimov, J Zhao, A V Nechaev, A Nadort, D Jin, T W Prow, M S Roberts, A V Zvyagin *J. Biomed. Opt*. **18** 061215 (2012)
36. S Heer, K Kömpe, H-U Güdel, M Haase *Adv. Mater*. **16** 2102 (2004)
37. H Li, L Wang *Chin. Sci. Bull*. **58** 4051 (2013)
38. Q Zhan, J Qian, H Liang, G Somesfalean, D Wang, S He, Z Zhang, S Andersson-Engels *ACS Nano* **5** 3744 (2011)
39. S Hao, G Chen, C Yang *Theranostics* **3** 331 (2013)
40. L Cheng, K Yang, S Zhang, M Shao, S Lee, Z Liu *Nano Res*. **3** 722 (2010)
41. J Lan, F Wen, F Fu, X Zhang, S Cai, Z Liu, D Wu, C Li, J H Chen, C Wang *RSC Adv*. **5** 18008 (2015)
42. X Wang, K Liu, G Yang, L Cheng, L He, Y Liu, Y Li, L Guo, Z Liu *Nanoscale* **6** 9198 (2014)
43. M Wang, Z Chen, W Zheng, H Zhu, S Lu, E Ma, D Tu, S Zhou, M Huang, X Chen *Nanoscale* **6** 8274 (2014)
44. Q Liu, Y Sun, T Yang, W Feng, C Li, F Li *J. Am. Chem. Soc*. **133** 17122 (2011)
45. I Kamińska, K Fronc, B Sikora, M Mouawad, A Siemiarczuk, M Szewczyk, K Sobczak, T Wojciechowski, W Zaleszczyk, R Minikayev, W Paszkowicz, P Stępień, P Dziawa, K Ciszak, D Piątkowski, S Maćkowski, M Kaliszewski, M Włodarski, J Młyńczak, K Kopczyński, M Łapiński, D Elbaum *RSC Adv*. **5** 78361 (2015)
46. J Zhao, D Jin, E P Schartner, Y Lu, Y Liu, A V Zvyagin, L Zhang, J M Dawes, P Xi, J A Piper, E M Goldys, T M Monro *Nat. Nanotechnol*. **8** 729 (2013)
47. A Nadort, V K A Sreenivasan, Z Song, E A Grebenik, A V Nechaev, V A Semchishen, V Y Panchenko, A V Zvyagin *PloS One* **8** e63292 (2013)
48. F Wang, Y Han, C S Lim, Y Lu, J Wang, J Xu, H Chen, C Zhang, M Hong, X Liu *Nature (London)* **463** 1061 (2010)
49. X-F Qiao, J-C Zhou, J-W Xiao, Y-F Wang, L-D Sun, C-H Yan *Nanoscale* **4** 4611 (2012)
50. J-C Boyer, M -P Manseau, J I Murray, F C J M van Veggel *Langmuir* **26** 1157 (2010)
51. L Wang, Y Zhang, Y Zhu *Nano Res*. **3** 317 (2010)
52. Y Sun, X Zhu, J Peng, F Li *ACS Nano* **7** 11290 (2013)
53. P Yuan, Y H Lee, M K Gnanasammandhan, Z Guan, Y Zhang, Q-H Xu *Nanoscale* **4** 5132 (2012)
54. W Deng, L Sudheendra, J Zhao, J Fu, D Jin, I M Kennedy, E M Goldys *Nanotechnology* **22** 325604 (2011)
55. P Ramasamy, P Chandra, S W Rhee, J Kim *Nanoscale* **5** 8711 (2013)
56. S Jiang, M K Gnanasammandhan, Y Zhang *J. R. Soc. Interface* **7** 3 (2010)
57. T Cao, T Yang, Y Gao, Y Yang, H Hu, F Li *Inorg. Chem. Commun*. **13** 392 (2010)
58. K Liu, X Liu, Q Zeng, Y Zhang, L Tu, T Liu, X Kong, Y Wang, F Cao, S A G Lambrechts, M C G Aalders, H Zhang *ACS Nano* **6** 4054 (2012)
59. D Li, B Dong, X Bai, Y Wang, H Song *J. Phys. Chem. C* **114** 8219 (2010)

60. F Wang, D K Chatterjee, Z Li, Y Zhang, X Fan, M Wang *Nanotechnology* **17** 5786 (2006)
61. D K Chatterjee, Z Yong *Nanomedicine (London)* **3** 73 (2008)
62. W Yang, Y Wang, L Chang, C Liu, J Bai, Z Li *RSC Adv.* **4** 14546 (2014)
63. L Xiong, T Yang, Y Yang, C Xu, F Li *Biomaterials* **31** 7078 (2010)
64. J Liu, Q Q Zhan, in *Progress in Electromagnetics Research Symposium (PIERS Proc.), Guangzhou, China, 2014* p. 2736
65. J Lee, T S Lee, J Ryu, S Hong, M Kang, K Im, J H Kang, S M Lim, S Park, R Song *J. Nucl. Med.* **54** 96 (2013)
66. L Wang, R Yan, Z Huo, L Wang, J Zeng, J Bao, X Wang, Q Peng, Y Li *Angew. Chem., Int. Ed.* **44** 6054 (2005)
67. C Wang, L Cheng, Y Liu, X Wang, X Ma, Z Deng, Y Li, Z Liu *Adv. Funct. Mater.* **23** 3077 (2013)
68. R A Jalil, Y Zhang *Biomaterials* **29** 4122 (2008)
69. X Ma, S Li, Y Xia, Z Wang *Anal. Lett.* **47** 2048 (2014)
70. B Chen, B Dong, J Wang, S Zhang, L Xu, W Yu, H Song *Nanoscale* **5** 8541 (2013)
71. Z Liu, L Sun, F Li, Q Liu, L Shi, D Zhang, S Yuan, T Liu, Y Qiu *J. Mater. Chem.* **21** 17615 (2011)
72. J Shan, J Chen, J Meng, J Collins, W Soboyejo, J S Friedberg, Y Ju *J. Appl. Phys.* **104** 094308 (2008)
73. A E Guller, A N Generalova, E V Petersen, A V Nechaev, I A Trusova, N N Landyshev, A Nadort, E A Grebenik, S M Deyev, A B Shekhter, A V Zvyagin *Nano Res.* **8** 1546 (2015)
74. A N Generalova, I K Kochneva, E V Khaydukov, V A Semchishen, A E Guller, A V Nechaev, A B Shekhter, V P Zubov, A V Zvyagin, S M Deyev *Nanoscale* **7** 1709 (2015)
75. E A Grebenik, A Nadort, A N Generalova, A V Nechaev, V K A Sreenivasan, E V Khaydukov, V A Semchishen, A P Popov, V I Sokolov, A S Akhmanov, V P Zubov, D V Klinov, V Y Panchenko, S M Deyev, A V Zvyagin *J. Biomed. Opt.* **18** 076004 (2013)
76. H Hu, M Yu, F Li, Z Chen, X Gao, L Xiong, C Huang *Chem. Mater.* **20** 7003 (2008)
77. X Ge, L Dong, L Sun, Z Song, R Wei, L Shi, H Chen *Nanoscale* **7** 7206 (2015)
78. Z Chen, H Chen, H Hu, M Yu, F Li, Q Zhang, Z Zhou, T Yi, C Huang *J. Am. Chem. Soc.* **130** 3023 (2008)
79. L Xiong, Z Chen, Q Tian, T Cao, C Xu, F Li *Anal. Chem.* **81** 8687 (2009)
80. F Alexis, E Pridgen, L K Molnar, O C Farokhzad *Mol. Pharm.* **5** 505 (2008)
81. J Lu, Y Chen, D Liu, W Ren, Y Lu, Y Shi, J Piper, I Paulsen, D Jin *Anal. Chem.* **87** 10406 (2015)
82. S Cui, D Yin, Y Chen, Y Di, H Chen, Y Ma, S Achilefu, Y Gu *ACS Nano* **7** 676 (2013)
83. D J Naczynski, T Andelman, D Pal, S Chen, R E Riman, C M Roth, P V Moghe *Small* **6** 1631 (2010)
84. D K Chatterjee, A J Rufaihah, Y Zhang *Biomaterials* **29** 937 (2008)
85. Y I Park, H M Kim, J H Kim, K C Moon, B Yoo, K T Lee, N Lee, Y Choi, W Park, D Ling, K Na, W K Moon, C S Hong, H S Park, S-Y Yoon, Y D Suh, H Lee, T Hyeon *Adv. Mater.* **24** 5755 (2012)
86. S F Lim, R Riehn, W S Ryu, N Khanarian, C-k Tung, D Tank, R H Austin *Nano Lett.* **6** 169 (2006)
87. W Di, J Li, N Shirahata, Y Sakka, M-G Willinger, N Pinna *Nanoscale* **3** 1263 (2011)
88. Y Wei, Q Chen, B Wu, A Zhou, D Xing *Nanoscale* **4** 3901 (2012)
89. J Zhou, Y Sun, X Du, L Xiong, H Hu, F Li *Biomaterials* **31** 3287 (2010)
90. D Tu, L Liu, Q Ju, Y Liu, H Zhu, R Li, X Chen *Angew. Chem., Int. Ed.* **50** 6306 (2011)
91. E Beaurepaire, V Buissette, M-P Sauviat, D Giaume, K Lahlil, A Mercuri, D Casanova, A Huignard, J-L Martin, T Gacoin, J-P Boilot, A Alexandrou *Nano Lett.* **4** 2079 (2004)
92. N M Idris, M K Gnanasammandhan, J Zhang, P C Ho, R Mahendran, Y Zhang *Nat. Med.* **18** 1580 (2012)
93. M Deng, Y Ma, S Huang, G Hu, L Wang *Nano Res.* **4** 685 (2011)
94. S H Nam, Y M Bae, Y I Park, J H Kim, H M Kim, J S Choi, K T Lee, T Hyeon, Y D Suh *Angew. Chem., Int. Ed.* **50** 6093 (2011)
95. M Nyk, R Kumar, T Y Ohulchanskyy, E J Bergey, P N Prasad *Nano Lett.* **8** 3834 (2008)
96. T Cao, Y Yang, Y Gao, J Zhou, Z Li, F Li *Biomaterials* **32** 2959 (2011)
97. H Maeda *Adv. Enzyme Regul.* **41** 189 (2001)
98. J Fang, H Nakamura, H Maeda *Adv. Drug Deliv. Rev.* **63** 136 (2011)
99. Z Liu, R Peng *Eur. J. Nucl. Med. Mol. Imag.* **37** 147 (2010)
100. N M Idris, Z Li, L Ye, E K W Sim, R Mahendran, P C-L Ho, Y Zhang *Biomaterials* **30** 5104 (2009)
101. J Jin, Z Xu, Y Zhang, Y-J Gu, M H-W Lam, W-T Wong *Adv. Healthcare Mater.* **2** 1501 (2013)
102. S Jiang, Y Zhang, K M Lim, E K W Sim, L Ye *Nanotechnology* **20** 155101 (2009)
103. Q Dou, N M Idris, Y Zhang *Biomaterials* **34** 1722 (2013)
104. G Yi, Y Peng, Z Gao *Chem. Mater.* **23** 2729 (2011)
105. E N Lebedenko, S M Deyev *Acta Naturae* **1** (1) 32 (2009)
106. S M Deyev, E N Lebedenko, L E Petrovskaya, D A Dolgikh, A G Gabibov, M P Kirpichnikov *Russ. Chem. Rev.* **84** 1 (2015)
107. Q Chen, X Wang, F Chen, Q Zhang, B Dong, H Yang, G Liu, Y Zhu *J. Mater. Chem.* **21** 7661 (2011)
108. L Cheng, K Yang, Y Li, J Chen, C Wang, M Shao, S-T Lee, Z Liu *Angew. Chem., Int. Ed.* **50** 7385 (2011)
109. C Wang, L Cheng, Z Liu *Biomaterials* **32** 1110 (2011)
110. H Hu, L Xiong, J Zhou, F Li, T Cao, C Huang *Chem. – Eur. J.* **15** 3577 (2009)
111. X Liu, I Que, X Kong, Y Zhang, L Tu, Y Chang, T T Wang, A Chan, C W G M Llwik, H Zhang *Nanoscale* **7** 14914 (2015)
112. L-Q Xiong, Z-G Chen, M-X Yu, F-Y Li, C Liu, C-H Huang *Biomaterials* **30** 5592 (2009)
113. Y Yuan, Y Min, Q Hu, B Xing, B Liu *Nanoscale* **6** 11259 (2014)
114. T Zako, H Nagata, N Terada, A Utsumi, M Sakono, M Yohda, H Ueda, K Soga, M Maeda *Biochem. Biophys. Res. Commun.* **381** 54 (2009)
115. X-F Yu, Z Sun, M Li, Y Xiang, Q-Q Wang, F Tang, Y Wu, Z Cao, W Li *Biomaterials* **31** 8724 (2010)
116. G Hu, W Sheng, Y Zhang, X Wu, S Wang *Anal. Bioanal. Chem.* **407** 8487 (2015)
117. H Wu, Q Huo, S Varnum, J Wang, G Liu, Z Nie, J Liu, Y Lin *Analyst* **133** 1550 (2008)
118. X Wu, H Liu, J Liu, K N Haley, J A Treadway, J P Larson, N Ge, F Peale, M P Bruchez *Nat. Biotechnol.* **21** 41 (2002)
119. E A Ivukina, V K A Sreenivasan, O A Stremovskiy, B V Veryugin, S V Lukash, A V Zvyagin, S M Deyev, R V Petrov *Dokl. Biochem. Biophys.* **440** 231 (2011)
120. L Wang, Y Li *Chem. Commun.* 2557 (2006)

121. C M Dundas, D Demonte, S Park *Appl. Microbiol. Biotechnol.* **97** 9343 (2013)
122. T Rantanen, M L Järvenpää, J Vuojola, K Kuningas, T Soukka *Angew. Chem., Int. Ed.* **47** 3811 (2008)
123. G Schreiber, in *Nuclease Methods and Protocols* (Ed. C H Schein) (Totowa, NJ: Humana Press, 2001) p. 213
124. U F Aghayeva, M P Nikitin, S V Lukash, S M Deyev *ACS Nano* **7** 950 (2013)
125. R Khurana, A T Hate, U Nath, J B Udgaonkar *Protein Sci.* **4** 1133 (1995)
126. T I Prior, D J FitzGerald, I Pastan *Cell* **64** 1017 (1991)
127. S M Deyev, R Waibel, E N Lebedenko, A P Schubiger, A Plückthun *Nat. Biotechnol.* **21** 1486 (2003)
128. M P Nikitin, T A Zdobnova, S V Lukash, O A Stremovskiy, S M Deyev *Proc. Natl. Acad. Sci. USA* **107** 5827 (2010)
129. E N Lebedenko, T G Balandin, E F Edelweiss, O Georgiev, E S Moiseeva, R V Petrov, S M Deyev *Dokl. Biochem. Biophys.* **414** 120 (2007)
130. V K A Sreenivasan, E A Ivukina, W Deng, T A Kelf, T A Zdobnova, S V Lukash, B V Veryugin, O A Stremovskiy, A V Zvyagin, S M Deyev *J. Mater. Chem.* **21** 65 (2011)
131. R J Palmer, J L Butenhoff, J B Stevens *Environ. Res.* **43** 142 (1987)
132. J Zhang, F Liu, T Li, X He, Z Wang *RSC Adv.* **5** 7773 (2015)
133. U Kostiv, O Janoušková, M Šlouf, N Kotov, H Engstová, K Smolková, P Ježek, D Horák *Nanoscale* **7** 18096 (2015)
134. K Liu, J A Holz, Y Ding, X Liu, Y Zhang, L Tu, X Kong, B Priem, A Nadort, S A G Lambrechts, M C G Aalders, W J Buma, Y Liu, H Zhang *Nanoscale* **7** 1596 (2015)
135. A Nadort, L Liang, E Grebenik, A Guller, Y Lu, Y Qian, E Goldys, A Zvyagin *Proc. SPIE – Int. Soc. Opt. Photon.* **9668** 96683Y (2015)
136. J Shan, S J Budijono, G Hu, N Yao, Y Kang, Y Ju, R K Prud'homme *Adv. Funct. Mater.* **21** 2488 (2011)
137. H Guo, N M Idris, Y Zhang *Langmuir* **27** 2854 (2011)
138. P Zhang, W Steelant, M Kumar, M Scholfield *J. Am. Chem. Soc.* **129** 4526 (2007)
139. Q Q Dou, C P Teng, E Ye, X J Loh *Int. J. Nanomed.* **10** 419 (2015)
140. M E Lim, Y-l Lee, Y Zhang, J J H Chu *Biomaterials* **33** 1912 (2012)
141. H S Qian, H C Guo, P C-L Ho, R Mahendran, Y Zhang *Small* **5** 2285 (2009)
142. H Ding, Y Lv, D Ni, J Wang, Z Tian, W Wei, G Ma *Nanoscale* **7** 9806 (2015)
143. C Wang, H Tao, L Cheng, Z Liu *Biomaterials* **32** 6145 (2011)
144. M Guan, H Dong, J Ge, D Chen, L Sun, S Li, C Wang, C Yan, P Wang, C Shu *NPG Asia Mater.* **7** Art. No. e205 (2015)
145. Y Ye, Y Li, F Fang *Int. J. Nanomed.* **9** 5157 (2014)